

RECEIVED: September 23, 2022

REVISED: February 26, 2023

ACCEPTED: March 4, 2023

PUBLISHED: March 17, 2023

Study of $\eta(1405)/\eta(1475)$ in $J/\psi \rightarrow \gamma K_S^0 K_S^0 \pi^0$ decay



The BESIII collaboration

E-mail: besiii-publications@ihep.ac.cn

ABSTRACT: Using a sample of $(10.09 \pm 0.04) \times 10^9$ J/ψ decays collected with the BESIII detector, partial wave analyses of the decay $J/\psi \rightarrow \gamma K_S^0 K_S^0 \pi^0$ are performed within the $K_S^0 K_S^0 \pi^0$ invariant mass region below $1.6 \text{ GeV}/c^2$. The covariant tensor amplitude method is used in both mass independent and mass dependent approaches. Both analysis approaches exhibit dominant pseudoscalar and axial vector components, and show good consistency for the other individual components. Furthermore, the mass dependent analysis reveals that the $K_S^0 K_S^0 \pi^0$ invariant mass spectrum for the pseudoscalar component can be well described with two isoscalar resonant states using relativistic Breit-Wigner model, i.e., the $\eta(1405)$ with a mass of $1391.7 \pm 0.7_{-0.3}^{+11.3} \text{ MeV}/c^2$ and a width of $60.8 \pm 1.2_{-12.0}^{+5.5} \text{ MeV}$, and the $\eta(1475)$ with a mass of $1507.6 \pm 1.6_{-32.2}^{+15.5} \text{ MeV}/c^2$ and a width of $115.8 \pm 2.4_{-10.9}^{+14.8} \text{ MeV}$. The first and second uncertainties are statistical and systematic, respectively. Alternate models for the pseudoscalar component are also tested, but the description of the $K_S^0 K_S^0 \pi^0$ invariant mass spectrum deteriorates significantly.

KEYWORDS: e^+e^- Experiments, Particle and Resonance Production, Spectroscopy

ARXIV EPRINT: [2209.11175](https://arxiv.org/abs/2209.11175)

Contents

1	Introduction	1
2	BESIII detector and Monte Carlo simulation	2
3	Event selection	3
4	Partial wave analysis	6
4.1	Analysis method	6
4.2	Mass independent PWA	8
4.3	Mass dependent PWA	12
5	Systematic uncertainties	17
6	Summary	21
A	Formulas of covariant tensor amplitudes	22
	The BESIII collaboration	27

1 Introduction

The non-abelian nature of quantum chromodynamics (QCD) predicts the existence of exotic states, such as glueballs, hybrids, and multiquarks states. The experimental confirmation of these states would provide fundamental information about QCD in the confinement regime and would be a direct test of the QCD theory. The radiative decays of charmonium are glue-rich processes and are considered to be excellent probes for the production of gluonic matter and light hadron structures. Much progress has been made in the past few decades, but many issues remain unresolved.

In the field of light hadron spectroscopy, one of the most interesting and disputed questions is the nature of the pseudoscalar structure with a mass around $1.4 \text{ GeV}/c^2$, the so-called “ ι ” state. The “ ι ” state was first observed in the J/ψ radiative decay to the $K\bar{K}\pi$ final state in the early 1980s by the Crystal Barrel [1] and Mark II [2] Collaborations. The structure has been subsequently confirmed by different experiments [3–11], and is often interpreted as the combination of two isoscalar resonant states, i.e., the $\eta(1405)$ and $\eta(1475)$ [12]. Pseudoscalar structures in the vicinity of $1.4 \text{ GeV}/c^2$ are also observed in the $\eta\pi\pi$, $\pi\pi\pi$ and γV (where V refers to vector meson) final states of J/ψ radiative decays, but with quite different lineshapes [13–18]. Consequently, whether or not these observed pseudoscalar structures are from the same origin is controversial.

From the theoretical point of view, the pseudoscalar nonet of ground states is well established, and the $\eta(1295)$ and $\eta(1475)$ are generally assigned to be the first radial excitations of the ground states η and η' , taking into account their production and decay properties [12]. It is very difficult to accommodate another pseudoscalar state with a mass around $1.4 \text{ GeV}/c^2$ in the quark model. Therefore, the possibility of an additional state with a non- $q\bar{q}$ nature [19–25] has been widely discussed. Meanwhile, there is still a long-standing controversy about whether or not the $\eta(1405)$ and $\eta(1475)$ are two separate states or just one pseudoscalar state, namely the $\eta(1440)$, in different decay modes. In refs. [26–29], a coherent phenomenological analysis of $\eta(1405/1475) \rightarrow K\bar{K}\pi$, $\eta\pi\pi$ and $\pi\pi\pi$ is performed by considering a triangle singularity mechanism (TSM), and it is concluded that only one pseudoscalar state is needed in this mass vicinity, and the distorted lineshape and shifted peak position in the different decay modes could be due to dynamic features within the TSM.

To solve the $\eta(1405/1475)$ puzzle and to pin down their nature, a precise and comprehensive measurement is prerequisite. The BESIII experiment has collected 10.09×10^9 J/ψ decays [30], which provides an excellent opportunity to explore the nature of the $\eta(1405/1475)$. Meanwhile, comparing to other decay modes, $J/\psi \rightarrow \gamma K_S^0 K_S^0 \pi^0$ is free of background from similar final states with one fewer or more photon, and can provide a much cleaner sample than the corresponding charged channels. This article presents a partial wave analysis (PWA) of the decay $J/\psi \rightarrow \gamma K_S^0 K_S^0 \pi^0$ based on the full J/ψ sample collected by the BESIII collaboration, where both mass dependent and independent approaches are performed. Both K_S^0 mesons are reconstructed from $\pi^+\pi^-$ and the π^0 meson is reconstructed from $\gamma\gamma$.

2 BESIII detector and Monte Carlo simulation

The BESIII detector [31] records the final state particles produced in symmetric e^+e^- collisions provided by the BEPCII storage ring [32] in the center-of-mass energy range from 2.0 to 4.95 GeV [33], with a peak luminosity of $1 \times 10^{33} \text{ cm}^{-2} \text{ s}^{-1}$ achieved at $\sqrt{s} = 3.77 \text{ GeV}$. The cylindrical core of the BESIII detector covers 93% of the full solid angle. From inner detectors to outer, it consists of a helium-based multilayer drift chamber (MDC), a plastic scintillator time-of-flight system (TOF), and a CsI(Tl) electromagnetic calorimeter (EMC), which are all enclosed in a superconducting solenoidal magnet providing a 1.0 T (0.9 T in 2012) magnetic field. The solenoid is supported by an octagonal flux-return yoke with resistive plate counter muon identification modules interleaved with steel. The charged-particle momentum resolution at $1 \text{ GeV}/c$ is 0.5%, and the dE/dx resolution is 6% for electrons from Bhabha scattering. The EMC measures photon energies with a resolution of 2.5% (5%) at 1 GeV in the barrel (end cap) region. The time resolution in the TOF barrel region is 68 ps, while that in the end cap region was initially 110 ps. The end cap TOF system was upgraded in 2015 with multi-gap resistive plate chamber technology, improving the time resolution to be 60 ps [34, 35].

Simulated data samples produced with a GEANT4-based Monte Carlo (MC) package [36], which includes the geometric description of the BESIII detector [37, 38] and the detector response, are used to optimize the event selection criteria, determine detection

efficiencies and estimate backgrounds. The simulation models the beam energy spread and initial state radiation in the e^+e^- annihilations with the generator KKMC [39, 40]. The signal MC sample for $J/\psi \rightarrow \gamma K_S^0 K_S^0 \pi^0$, with subsequent decays $K_S^0 \rightarrow \pi^+ \pi^-$ and $\pi^0 \rightarrow \gamma \gamma$, is generated uniformly in phase space (PHSP).

An inclusive MC sample with 10.01×10^9 J/ψ decays is used to study background, where the production of the J/ψ resonance and the continuum processes is incorporated in KKMC [39, 40]. All particle decays are modeled with EVTGEN [41, 42] using branching fractions either taken from the Particle Data Group (PDG) [12], when available, or otherwise estimated with LUNDCHARM [43, 44]. Final state radiation from charged final state particles is incorporated using PHOTOS [45].

3 Event selection

Charged tracks are reconstructed using hits in the MDC. The point of closest approach of each charged track to the interaction point (IP) is required to be less than 20 cm along the z axis, which is the symmetry axis of the MDC, because of the relatively long lifetime of K_S^0 . Charged tracks detected in the MDC are required to be within a polar angle (θ) range of $|\cos \theta| < 0.93$, where θ is defined with respect to the z axis. All charged tracks are reconstructed under the pion hypothesis. To reconstruct K_S^0 candidates, a vertex fit and a subsequent secondary vertex fit are performed on each pair of charged tracks with opposite charges. When two vertex fits are performed successfully, the corresponding combination is regarded as an K_S^0 candidate. Photon candidates are identified using showers in the EMC. The deposited energy of each shower must be more than 25 MeV in the EMC barrel region ($|\cos \theta| < 0.80$) and more than 50 MeV in the end cap region ($0.86 < |\cos \theta| < 0.92$). To exclude those showers originating from charged tracks, the angle between the position of each shower in the EMC and the closest extrapolated charged track must be greater than 10° as measured from the IP. To suppress electronic noise and energy deposits unrelated to the event, the difference between the EMC time and the event start time is required to be within $[0, 700]$ ns.

In $J/\psi \rightarrow \gamma K_S^0 K_S^0 \pi^0$ process, candidates are required to have four charged tracks with zero net charge and at least three photon candidates. The K_S^0 candidates are required to satisfy $L/\sigma_L > 2$, where L and σ_L are the distance of the common vertex of the $\pi^+ \pi^-$ pair away from the IP, and the corresponding uncertainty, respectively. The $\gamma \gamma \gamma K_S^0 K_S^0$ candidates are further subjected to a four-constraint (4C) kinematic fit, which ensures energy and momentum conservation. Only candidates which yield a χ_{4C}^2 of the 4C kinematic fit of less than 40 are retained for further analysis. For events with more than three photon candidates, multiple signal candidates are possible, and only the one with the smallest χ_{4C}^2 is retained for further analysis. Furthermore, the $J/\psi \rightarrow \gamma K_S^0 K_S^0 \pi^0$ candidates are required to have exactly one pair of photons with invariant mass within the π^0 mass region ($|M(\gamma\gamma) - M(\pi^0)| < 20 \text{ MeV}/c^2$) [12], as shown in figure 1(a). MC simulation studies indicate this criterion significantly reduces the rate of miscombined photon pairs to be less than 0.3%. Both K_S^0 candidates are required to satisfy $|M(\pi^+ \pi^-) - M(K_S^0)| < 12 \text{ MeV}/c^2$, where $M(K_S^0)$ is the known K^0 mass [12], as shown in figures 1(b)-(c). The miscombination

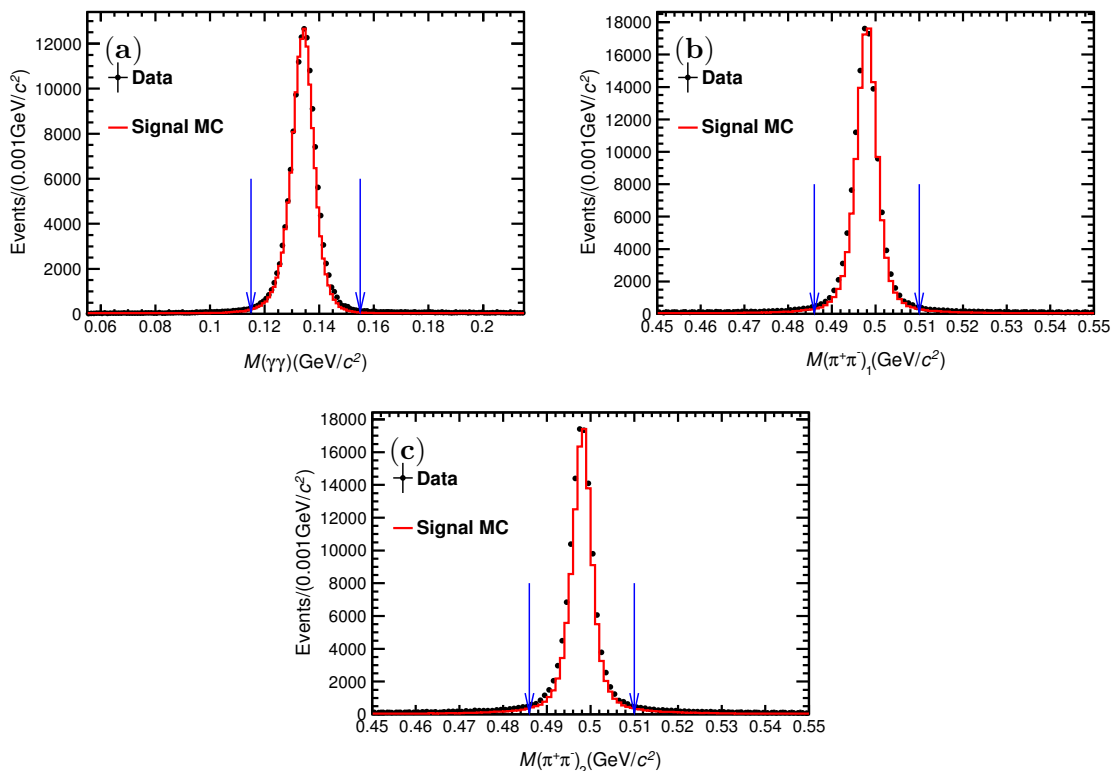


Figure 1. Invariant mass distributions of (a) $\gamma\gamma$, (b) one $\pi^+\pi^-$ pair, (c) another $\pi^+\pi^-$ pair for candidate events with the 4C kinematic fit applied. Dots with error bars are data and the red solid line represents the signal MC sample (normalized by height).

of pion pairs to form a K_S^0 signal is also studied and found to be negligible. To suppress backgrounds containing an η signal, events with any photon pair of invariant mass within ± 30 MeV/ c^2 of the known η mass [12] are rejected, while the efficiency for real signal is about 90.5%. The decay $J/\psi \rightarrow \omega K_S^0 K_S^0$ with $\omega \rightarrow \gamma\pi^0$ is of the same final state as the signal decay $J/\psi \rightarrow \gamma K_S^0 K_S^0 \pi^0$. Therefore, events with $\gamma\pi^0$ invariant mass within ± 40 MeV/ c^2 of the known ω mass [12] are rejected, while the efficiency for real signal is about 95.5%. After all the above selection criteria, potential backgrounds are studied by subjecting the inclusive MC sample of 10.01×10^9 J/ψ decays to the same selection criteria applied to data. No significant peaking background is identified in the invariant mass spectrum of $K_S^0 K_S^0 \pi^0$. The dominant background stemming from non- $K_S^0 K_S^0$ processes is estimated to be 0.5% in total. Non- $K_S^0 K_S^0$ backgrounds are estimated using events from $K_S^0 K_S^0$ two-dimensional sidebands from data, where the sideband regions are defined as $|M(\pi^+\pi^-)_{1,2} - M(K_S^0) \pm 35 \text{ MeV}/c^2| < 12 \text{ MeV}/c^2$, and the subscripts 1 and 2 stand for the two sets of $\pi^+\pi^-$ corresponding to the two K_S^0 . The total contribution is estimated to be at a level of 0.2%, which is neglected in the following analysis.

To improve the resolution of kinematic variables, the remaining $J/\psi \rightarrow \gamma K_S^0 K_S^0 \pi^0$ events are subjected to a seven-constraint (7C) kinematic fit, which, in addition to imposing energy and momentum conservation, further constrains the one π^0 and two K_S^0

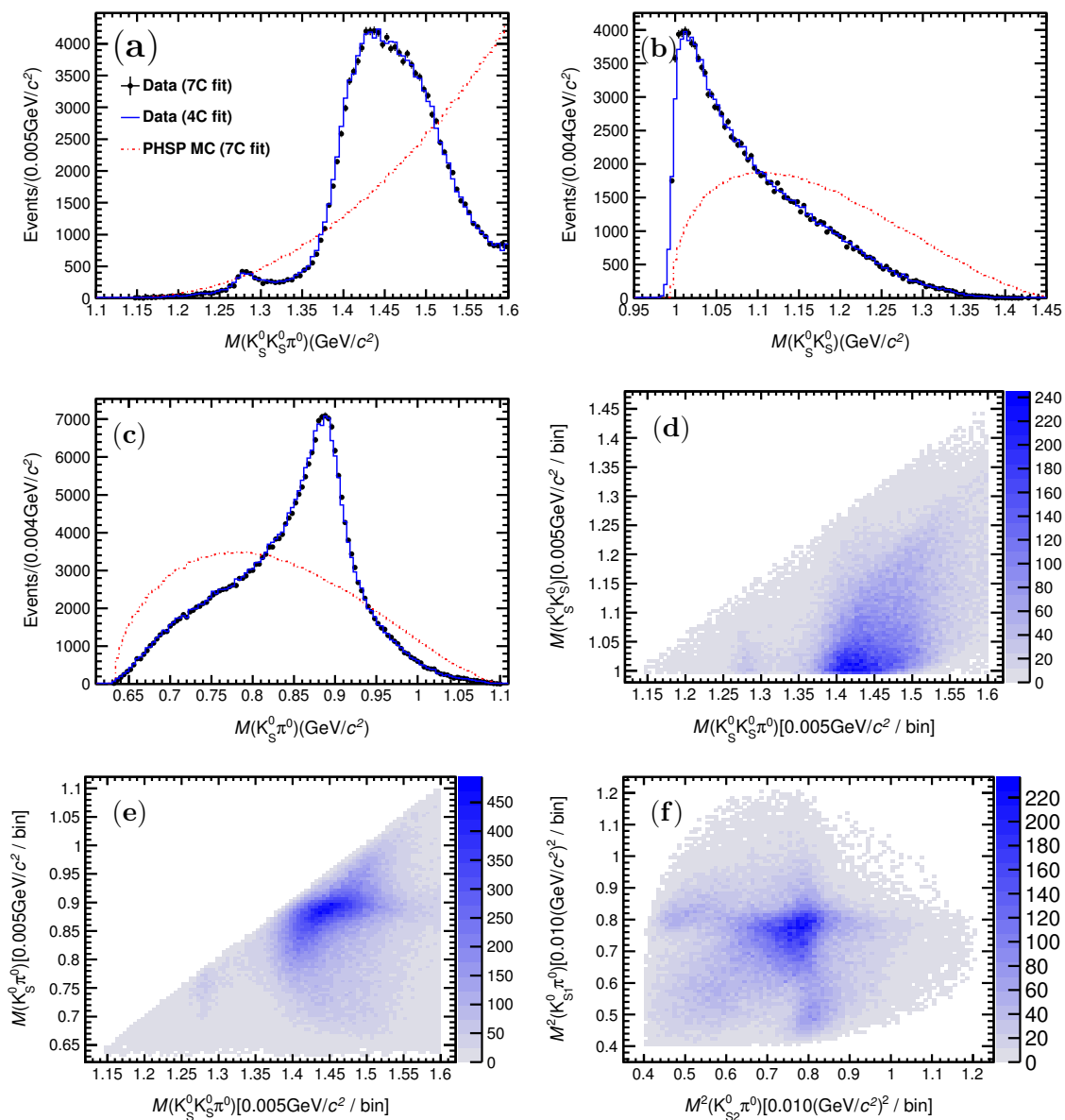


Figure 2. Invariant mass spectra of (a) $K_S^0 K_S^0 \pi^0$, (b) $K_S^0 K_S^0$, and (c) $K_S^0 \pi^0$ for events with the requirement $M(K_S^0 K_S^0 \pi^0) < 1.6 \text{ GeV}/c^2$. The corresponding two-dimensional distributions of (d) $M(K_S^0 K_S^0)$ versus $M(K_S^0 K_S^0 \pi^0)$ and (e) $M(K_S^0 \pi^0)$ versus $M(K_S^0 K_S^0 \pi^0)$. The corresponding Dalitz plot of (f) $M^2(K_{S1}^0 \pi^0)$ versus $M^2(K_{S2}^0 \pi^0)$. Dots with error bars are the data with the 7C kinematic fit applied. The blue solid line and the red dotted line represent the data with the 4C kinematic fit applied and the signal PHSP MC samples with the 7C kinematic fit applied (normalized by integral), respectively.

masses to their known values quoted in the PDG [12]. Detailed MC simulation studies show that the 7C kinematic fit improves the resolution of the $K_S^0 K_S^0 \pi^0$ invariant mass from $8.4 \text{ MeV}/c^2$ to $4.9 \text{ MeV}/c^2$ at $1.45 \text{ GeV}/c^2$, while the efficiency is more than 99.5%. After all the above criteria are imposed, the invariant mass spectrum of $K_S^0 K_S^0 \pi^0$ up to $1.6 \text{ GeV}/c^2$ is shown in figure 2(a) for data and the signal PHSP MC sample. A prominent structure around $1.45 \text{ GeV}/c^2$ as well as a clear bump around $1.28 \text{ GeV}/c^2$ are observed. The corresponding spectra of $K_S^0 K_S^0$ and $K_S^0 \pi^0$ invariant mass are presented in figures 2(b) and (c), respectively. The spectra reveal strong enhancements near the $K_S^0 K_S^0$ mass threshold and around $0.90 \text{ GeV}/c^2$ in the $K_S^0 \pi^0$ mass spectrum. The two-dimensional distributions of the invariant mass of $K_S^0 K_S^0 \pi^0$ versus that of $K_S^0 K_S^0$ and $K_S^0 \pi^0$ are also shown in figures 2(d) and (e), respectively. The Dalitz plot of $M^2(K_{S1}^0 \pi^0)$ versus $M^2(K_{S2}^0 \pi^0)$ for the selected candidates is shown in figure 2(f).

4 Partial wave analysis

4.1 Analysis method

Using the GPUPWA framework [46], a PWA is performed on the remaining 126,436 events in the region $M(K_S^0 K_S^0 \pi^0) < 1.6 \text{ GeV}/c^2$ in order to disentangle the structures present in the $K_S^0 K_S^0 \pi^0$ invariant mass spectrum. The quasi-two-body decay amplitudes in the decay process $J/\psi \rightarrow \gamma R_1$ with two sequential decays $R_1 \rightarrow K_S^0 R_2 \rightarrow K_S^0 K_S^0 \pi^0$ and $R_1 \rightarrow R_2 \pi^0 \rightarrow K_S^0 K_S^0 \pi^0$ are considered and constructed using the covariant tensor amplitudes described in ref. [47], where R_1 and R_2 are the intermediate states that can decay to $K_S^0 K_S^0 \pi^0$, $K_S^0 \pi^0$ or $K_S^0 K_S^0$, respectively.

Let A_X be the amplitude for a decay mode X , which has N_{W_X} independent partial wave amplitudes. For the J/ψ radiative decay, the general form of the A_X decay amplitude is:

$$A_X = \psi_\mu(m_1) e_\nu^*(m_2) \sum_{j=1}^{N_{W_X}} \Lambda_j U_j^{\mu\nu}, \quad (4.1)$$

according to ref. [47], where $\psi_\mu(m_1)$ is the polarization four-vector for the J/ψ ; $e_\nu(m_2)$ is the polarization four-vector for the photon; m_1 and m_2 are the spin projections of the J/ψ and photon, respectively; $U_j^{\mu\nu}$ is the j^{th} independent partial wave amplitude of J/ψ radiative decay by the mode X with coupling strength determined by a complex parameter Λ_j . The partial wave amplitudes $U_j^{\mu\nu}$ used in the analysis are constructed with the four-momenta of the particles in the final state, and their specific expressions are given in ref. [47].

The ordinary intermediate resonance is parametrized by a relativistic Breit-Wigner (BW) propagator with a constant-width

$$BW(s) = \frac{1}{M^2 - s - iM\Gamma}, \quad (4.2)$$

where s is the invariant mass squared of resonances, M and Γ are the corresponding mass and width.

For $a_0(980)^0$ with mass near $K\bar{K}$ threshold, we use dispersion integrals to describe its lineshape, following the prescription given in ref. [48]. The $a_0(980)^0$ amplitude is constructed using the following denominator:

$$D_\alpha(s) = m_0^2 - s - \sum_{ch} \Pi_{ch}(s), \quad (4.3)$$

where m_0 is the $a_0(980)$ mass and $\Pi_{ch}(s)$ in the sum over channels is a complex function, with imaginary part

$$\text{Im}\Pi_{ch}(s) = g_{ch}^2 \rho_{ch}(s) F_{ch}(s), \quad (4.4)$$

while real parts are given by principal value integrals,

$$\text{Re}\Pi_{ch}(s) = \frac{1}{\pi} P \int_{s_{ch}}^{\infty} \frac{\text{Im}\Pi_{ch}(s') ds'}{(s' - s)}. \quad (4.5)$$

In the above expressions $\rho_{ch}(s)$ is the available phase space for a given channel, obtained from the corresponding decay momentum $q_{ch}(s)$. The integral in eq. (4.5) is divergent when $s \rightarrow \infty$, so the phase space is modified by a form factor $F_{ch}(s) = e^{-\beta q_{ch}^2(s)}$, where the parameter β is related to the root-mean-square size of an emitting source [48]. We consider three $a_0(980)^0$ decay channels here, the $\pi\eta$, $K\bar{K}$, and $\eta'\pi$, with corresponding coupling constants and the value of $a_0(980)^0$ mass quoted from ref. [49].

The complex coefficients of the amplitudes and resonance parameters are determined by an unbinned maximum likelihood fit to the data. The likelihood function is constructed following a method similar to that used in ref. [50].

The probability to observe the i^{th} event characterized by the measurement ξ_i , i.e., the measured four-momenta of the particles in the final state, is:

$$P(\xi_i) = \frac{|M(\xi_i)|^2 \epsilon(\xi_i) \Phi(\xi_i)}{\sigma'}, \quad (4.6)$$

where $\epsilon(\xi_i)$ is the detection efficiency, $\Phi(\xi_i)$ is the standard element of phase space, and $M(\xi_i) = \sum_X A_X(\xi_i)$ is the matrix element describing the decay processes from the J/ψ to the final state $\gamma K_S^0 K_S^0 \pi^0$. $A_X(\xi_i)$ is the amplitude corresponding to decay mode X as defined in eq. (4.1) and $\sigma' \equiv \int |M(\xi)|^2 \epsilon(\xi) \Phi(\xi) d\xi$ is the normalization integral.

The joint probability for observing N events in the data sample is:

$$\mathcal{L} = \prod_{i=1}^N P(\xi_i) = \prod_{i=1}^N \frac{|M(\xi_i)|^2 \epsilon(\xi_i) \Phi(\xi_i)}{\sigma'}. \quad (4.7)$$

For technical reasons, rather than maximizing \mathcal{L} , $\mathcal{S} = -\ln \mathcal{L}$ is minimized, with

$$\mathcal{S} = -\ln \mathcal{L} = -\sum_{i=1}^N \ln |M(\xi_i)|^2 + N \ln \sigma' - \sum_{i=1}^N \ln \epsilon(\xi_i) \Phi(\xi_i), \quad (4.8)$$

For a given data set. The third term is a constant and has no impact on the determination of the parameters of the amplitudes or on the relative changes of $-\ln \mathcal{L}$ values. In the fitting, the third term will not be considered.

The free parameters are optimized by MINUIT [51]. The normalization integral σ' is evaluated using MC techniques. A signal PHSP MC sample of N_{gen} events is generated. These events are put through the detector simulation, subjected to the selection criteria and yield a sample of N_{acc} accepted events. The normalization integral is computed as:

$$\sigma' = \int |M(\xi)|^2 \epsilon(\xi) \Phi(\xi) d\xi \rightarrow \frac{1}{N_{\text{gen}}} \sum_{j=1}^{N_{\text{acc}}} |M(\xi_j)|^2, \quad (4.9)$$

where the constant value of the phase space integral $\int \Phi(\xi) d\xi$ is ignored.

The number of the fitted events N_X for a decay mode X , which has N_{W_X} independent decay amplitudes, is defined as:

$$N_X = \frac{\sigma_X}{\sigma'} \cdot N, \quad (4.10)$$

where N is the number of selected events after background subtraction, and

$$\sigma_X = \frac{1}{N_{\text{gen}}} \sum_{j=1}^{N_{\text{acc}}} |A_X(\xi_j)|^2, \quad (4.11)$$

is calculated with the same MC sample as the normalization integral σ' .

The branching fraction of a decay mode X is calculated as:

$$\mathcal{B} = \frac{N_X}{N_{J/\psi} \cdot \epsilon_X \cdot \mathcal{B}_{K_S^0 \rightarrow \pi^+ \pi^-}^2 \cdot \mathcal{B}_{\pi^0 \rightarrow \gamma \gamma}}, \quad (4.12)$$

where the detection efficiency ϵ_X for the decay mode X is obtained by the partial wave amplitude weighted MC sample,

$$\epsilon_X = \frac{\sigma_X}{\sigma_X^{\text{gen}}} = \frac{\sum_{k=1}^{N_{\text{acc}}} |A_X(\xi_k)|^2}{\sum_{j=1}^{N_{\text{gen}}} |A_X(\xi_j)|^2}, \quad (4.13)$$

N_X is the number of the fitted events for the decay mode X ; $N_{J/\psi} = (10.09 \pm 0.04) \times 10^9$ is the total number of J/ψ events [30]; $\mathcal{B}_{K_S^0 \rightarrow \pi^+ \pi^-} = (69.2 \pm 0.05)\%$ and $\mathcal{B}_{\pi^0 \rightarrow \gamma \gamma} = (98.823 \pm 0.034)\%$ are the branching fractions of $K_S^0 \rightarrow \pi^+ \pi^-$ and $\pi^0 \rightarrow \gamma \gamma$ quoted from ref. [12], respectively. Additionally, the branching fractions are defined as the coherent sum over the $R_1 \rightarrow K_{S1}^0 R_2 \rightarrow K_{S1}^0 K_{S2}^0 \pi^0$ and $R_1 \rightarrow K_{S2}^0 R_2 \rightarrow K_{S2}^0 K_{S1}^0 \pi^0$ contributions for $J/\psi \rightarrow \gamma R_1, R_1 \rightarrow K_S^0 R_2 \rightarrow K_S^0 K_S^0 \pi^0$ processes in this analysis.

4.2 Mass independent PWA

To investigate the contributions from different components, a mass independent (MI) PWA is performed, which is mandatory in order to explore the lineshape of the $K_S^0 K_S^0 \pi^0$ invariant mass distribution for the different decay modes, and to minimize the bias from a particular model for the dynamics of the intermediate states.

In practice, a MI PWA where the intermediate states in the $K_S^0 K_S^0 \pi^0$ invariant mass spectrum are parameterized by a separate complex constant for each of 24 bins of 15 MeV/ c^2 width, while the part of the amplitude that describes the dynamical function is constant

J^{PC}	0^{-+}	1^{++}	1^{-+}	2^{++}	2^{-+}
for $K_S^0 \pi^0$	$K^*(892)^0 K_S^0$ $(K_S^0 \pi^0)_{\text{P-phsp}} K_S^0$ $(K_S^0 \pi^0)_{\text{D-phsp}} K_S^0$ $K_0^*(700)^0 K_S^0$ $(K_S^0 \pi^0)_{\text{S-phsp}} K_S^0$	$K^*(892)^0 K_S^0$ $(K_S^0 \pi^0)_{\text{P-phsp}} K_S^0$ $(K_S^0 \pi^0)_{\text{D-phsp}} K_S^0$ $K_0^*(700)^0 K_S^0$ $(K_S^0 \pi^0)_{\text{S-phsp}} K_S^0$	$K^*(892)^0 K_S^0$ $(K_S^0 \pi^0)_{\text{P-phsp}} K_S^0$ $(K_S^0 \pi^0)_{\text{D-phsp}} K_S^0$	$K^*(892)^0 K_S^0$ $(K_S^0 \pi^0)_{\text{P-phsp}} K_S^0$ $(K_S^0 \pi^0)_{\text{D-phsp}} K_S^0$	$K^*(892)^0 K_S^0$ $(K_S^0 \pi^0)_{\text{P-phsp}} K_S^0$ $(K_S^0 \pi^0)_{\text{D-phsp}} K_S^0$ $K_0^*(700)^0 K_S^0$ $(K_S^0 \pi^0)_{\text{S-phsp}} K_S^0$
for $K_S^0 K_S^0$	$a_2(1320)^0 \pi^0$ $(K_S^0 K_S^0)_{\text{D-phsp}} \pi^0$ $a_0(980)^0 \pi^0$ $a_0(1450)^0 \pi^0$ $(K_S^0 K_S^0)_{\text{S-phsp}} \pi^0$	$a_2(1320)^0 \pi^0$ $(K_S^0 K_S^0)_{\text{D-phsp}} \pi^0$ $a_0(980)^0 \pi^0$ $a_0(1450)^0 \pi^0$ $(K_S^0 K_S^0)_{\text{S-phsp}} \pi^0$	$a_2(1320)^0 \pi^0$ $(K_S^0 K_S^0)_{\text{D-phsp}} \pi^0$	$a_2(1320)^0 \pi^0$ $(K_S^0 K_S^0)_{\text{D-phsp}} \pi^0$	$a_2(1320)^0 \pi^0$ $(K_S^0 K_S^0)_{\text{D-phsp}} \pi^0$ $a_0(980)^0 \pi^0$ $a_0(1450)^0 \pi^0$ $(K_S^0 K_S^0)_{\text{S-phsp}} \pi^0$

Table 1. The set of all possible decay mode candidates evaluated in the MI PWA.

over a small range of s , is performed in the region $M(K_S^0 K_S^0 \pi^0) < 1.6 \text{ GeV}/c^2$ to extract the contribution of components with different decay modes, this method also has been described as “Bin-by-bin analysis” in ref. [52]. Taking into account the spin-parity, charge conjugation and isospin conservation, all possible decay mode candidates are evaluated, as listed in table 1, where “S”, “P” and “D” represent the mother resonance decaying with orbital angular momentum equal to 0, 1 and 2, respectively. The “phsp” refers to the direct decay process without an intermediate resonance, and is modeled by the corresponding PHSP distribution without a propagator. Only the partial wave amplitudes with smallest orbital angular momentum are considered in the analysis because of the strong suppression on the magnitude from the centrifugal barrier [47] for large orbital angular momentum waves. In the fit, all resonance parameters are fixed to the PDG values [12] or published results [49]. The changes on the negative log-likelihood (NLL) value and the number of free parameters in the fits with and without a component are used to evaluate its statistical significance. The nominal solution, in which the significance of each component is greater than 5σ , is retained as the baseline in each bin.

In the MI PWA results, the fit components of the nominal solutions for 24 bins are shown in table 2. The $K_S^0 K_S^0 \pi^0$ intensity spectra obtained from the MI PWA results are shown in figure 3, where $(K_S^0 K_S^0)_{\text{S-wave}} \pi^0$ represents the combination of $a_0(980)^0 \pi^0$ and $(K_S^0 K_S^0)_{\text{S-phsp}} \pi^0$ waves, and $(K_S^0 \pi^0)_{\text{P-wave}} K_S^0$ represents the combination of $K^*(892)^0 K_S^0$ and $(K_S^0 \pi^0)_{\text{P-phsp}} K_S^0$ waves. The fit results confirm that the pseudoscalar component is the dominant contribution. However, unlike a general resonance, the lineshape of the total pseudoscalar component does not exhibit an obvious peak position. It is instead relatively constant between $1.4 \text{ GeV}/c^2$ and $1.5 \text{ GeV}/c^2$. Further analysis shows that the pseudoscalar component decays into the $(K_S^0 K_S^0)_{\text{S-wave}} \pi^0$ and $(K_S^0 \pi^0)_{\text{P-wave}} K_S^0$ partial waves are of comparable magnitudes, but with different lineshapes and peaks. Axial vector components also contribute prominently, peaking at $1.28 \text{ GeV}/c^2$ and $1.42 \text{ GeV}/c^2$, respectively, and the corresponding component peaking at $1.28 \text{ GeV}/c^2$ decays into $a_0(980)^0 \pi^0$, while that peaking at $1.42 \text{ GeV}/c^2$ into $K^*(892)^0 K_S^0$. There is also a small tensor component decaying into $K^*(892)^0 K_S^0$ around $1.52 \text{ GeV}/c^2$, which is observed in the decay of $J/\psi \rightarrow \gamma K \bar{K} \pi$ for the first time.

1.240–1.255 GeV/c ²	1.255–1.270 GeV/c ²	1.270–1.285 GeV/c ²	1.285–1.300 GeV/c ²	1.300–1.315 GeV/c ²	1.315–1.330 GeV/c ²	1.330–1.345 GeV/c ²	1.345–1.360 GeV/c ²	1.360–1.375 GeV/c ²	1.375–1.390 GeV/c ²	1.390–1.405 GeV/c ²	1.405–1.420 GeV/c ²
0 ⁺ → a ₀ (980) ⁰ π ⁰	0 ⁺ → a ₀ (980) ⁰ π ⁰	0 ⁺ → a ₀ (980) ⁰ π ⁰	0 ⁺ → a ₀ (980) ⁰ π ⁰	0 ⁺ → a ₀ (980) ⁰ π ⁰	0 ⁺ → a ₀ (980) ⁰ π ⁰	0 ⁺ → a ₀ (980) ⁰ π ⁰	0 ⁺ → a ₀ (980) ⁰ π ⁰	0 ⁺ → a ₀ (980) ⁰ π ⁰	0 ⁺ → a ₀ (980) ⁰ π ⁰	0 ⁺ → a ₀ (980) ⁰ π ⁰	0 ⁺ → a ₀ (980) ⁰ π ⁰
0 ⁺ → K ⁺ (892) ⁰ K _S ⁰	0 ⁺ → K ⁺ (892) ⁰ K _S ⁰	0 ⁺ → K ⁺ (892) ⁰ K _S ⁰	0 ⁺ → K ⁺ (892) ⁰ K _S ⁰	0 ⁺ → K ⁺ (892) ⁰ K _S ⁰	0 ⁺ → K ⁺ (892) ⁰ K _S ⁰	0 ⁺ → K ⁺ (892) ⁰ K _S ⁰	0 ⁺ → K ⁺ (892) ⁰ K _S ⁰	0 ⁺ → K ⁺ (892) ⁰ K _S ⁰	0 ⁺ → K ⁺ (892) ⁰ K _S ⁰	0 ⁺ → K ⁺ (892) ⁰ K _S ⁰	0 ⁺ → K ⁺ (892) ⁰ K _S ⁰
1 ⁺⁺ → a ₀ (980) ⁰ π ⁰	1 ⁺⁺ → a ₀ (980) ⁰ π ⁰	1 ⁺⁺ → a ₀ (980) ⁰ π ⁰	1 ⁺⁺ → a ₀ (980) ⁰ π ⁰	1 ⁺⁺ → a ₀ (980) ⁰ π ⁰	1 ⁺⁺ → a ₀ (980) ⁰ π ⁰	1 ⁺⁺ → a ₀ (980) ⁰ π ⁰	1 ⁺⁺ → a ₀ (980) ⁰ π ⁰	1 ⁺⁺ → a ₀ (980) ⁰ π ⁰	1 ⁺⁺ → a ₂ (1320) ⁰ π ⁰	1 ⁺⁺ → a ₂ (1320) ⁰ π ⁰	1 ⁺⁺ → a ₂ (1320) ⁰ π ⁰
									0 ⁺ → (K _S ⁰ π ⁰) _{ρ±,ρ∓,π⁰} K _S ⁰	0 ⁺ → (K _S ⁰ π ⁰) _{ρ±,ρ∓,π⁰} K _S ⁰	0 ⁺ → (K _S ⁰ π ⁰) _{ρ±,ρ∓,π⁰} K _S ⁰
									0 ⁺ → (K _S ⁰ K _S ⁰) _{ρ±,ρ∓,π⁰}	0 ⁺ → (K _S ⁰ K _S ⁰) _{ρ±,ρ∓,π⁰}	0 ⁺ → (K _S ⁰ K _S ⁰) _{ρ±,ρ∓,π⁰}
									1 ⁺⁺ → K ⁺ (892) ⁰ K _S ⁰	1 ⁺⁺ → K ⁺ (892) ⁰ K _S ⁰	1 ⁺⁺ → K ⁺ (892) ⁰ K _S ⁰

1.420–1.435 GeV/c ²	1.435–1.450 GeV/c ²	1.450–1.465 GeV/c ²	1.465–1.480 GeV/c ²	1.480–1.495 GeV/c ²	1.495–1.510 GeV/c ²	1.510–1.525 GeV/c ²	1.525–1.540 GeV/c ²	1.540–1.555 GeV/c ²	1.555–1.570 GeV/c ²	1.570–1.585 GeV/c ²	1.585–1.600 GeV/c ²
0 ⁺ → a ₀ (980) ⁰ π ⁰	0 ⁺ → a ₀ (980) ⁰ π ⁰	0 ⁺ → a ₀ (980) ⁰ π ⁰	0 ⁺ → a ₀ (980) ⁰ π ⁰	0 ⁺ → a ₀ (980) ⁰ π ⁰	0 ⁺ → a ₀ (980) ⁰ π ⁰	0 ⁺ → a ₀ (980) ⁰ π ⁰	0 ⁺ → a ₀ (980) ⁰ π ⁰	0 ⁺ → a ₀ (980) ⁰ π ⁰	0 ⁺ → a ₀ (980) ⁰ π ⁰	0 ⁺ → a ₀ (980) ⁰ π ⁰	0 ⁺ → a ₀ (980) ⁰ π ⁰
0 ⁺ → K ⁺ (892) ⁰ K _S ⁰	0 ⁺ → K ⁺ (892) ⁰ K _S ⁰	0 ⁺ → K ⁺ (892) ⁰ K _S ⁰	0 ⁺ → K ⁺ (892) ⁰ K _S ⁰	0 ⁺ → K ⁺ (892) ⁰ K _S ⁰	0 ⁺ → K ⁺ (892) ⁰ K _S ⁰	0 ⁺ → K ⁺ (892) ⁰ K _S ⁰	0 ⁺ → K ⁺ (892) ⁰ K _S ⁰	0 ⁺ → K ⁺ (892) ⁰ K _S ⁰	0 ⁺ → K ⁺ (892) ⁰ K _S ⁰	0 ⁺ → K ⁺ (892) ⁰ K _S ⁰	0 ⁺ → K ⁺ (892) ⁰ K _S ⁰
0 ⁺ → a ₂ (1320) ⁰ π ⁰	0 ⁺ → a ₂ (1320) ⁰ π ⁰	0 ⁺ → a ₂ (1320) ⁰ π ⁰	0 ⁺ → a ₂ (1320) ⁰ π ⁰	0 ⁺ → a ₂ (1320) ⁰ π ⁰	0 ⁺ → a ₂ (1320) ⁰ π ⁰	0 ⁺ → a ₂ (1320) ⁰ π ⁰	0 ⁺ → a ₂ (1320) ⁰ π ⁰	0 ⁺ → a ₂ (1320) ⁰ π ⁰	0 ⁺ → a ₂ (1320) ⁰ π ⁰	0 ⁺ → a ₂ (1320) ⁰ π ⁰	0 ⁺ → a ₂ (1320) ⁰ π ⁰
0 ⁺ → (K _S ⁰ π ⁰) _{ρ±,ρ∓,π⁰} K _S ⁰	0 ⁺ → (K _S ⁰ π ⁰) _{ρ±,ρ∓,π⁰} K _S ⁰	0 ⁺ → (K _S ⁰ π ⁰) _{ρ±,ρ∓,π⁰} K _S ⁰	0 ⁺ → (K _S ⁰ π ⁰) _{ρ±,ρ∓,π⁰} K _S ⁰	0 ⁺ → (K _S ⁰ π ⁰) _{ρ±,ρ∓,π⁰} K _S ⁰	0 ⁺ → (K _S ⁰ π ⁰) _{ρ±,ρ∓,π⁰} K _S ⁰	0 ⁺ → (K _S ⁰ π ⁰) _{ρ±,ρ∓,π⁰} K _S ⁰	0 ⁺ → (K _S ⁰ π ⁰) _{ρ±,ρ∓,π⁰} K _S ⁰	0 ⁺ → (K _S ⁰ π ⁰) _{ρ±,ρ∓,π⁰} K _S ⁰	0 ⁺ → (K _S ⁰ π ⁰) _{ρ±,ρ∓,π⁰} K _S ⁰	0 ⁺ → (K _S ⁰ π ⁰) _{ρ±,ρ∓,π⁰} K _S ⁰	0 ⁺ → (K _S ⁰ π ⁰) _{ρ±,ρ∓,π⁰} K _S ⁰
0 ⁺ → (K _S ⁰ K _S ⁰) _{ρ±,ρ∓,π⁰}	0 ⁺ → (K _S ⁰ K _S ⁰) _{ρ±,ρ∓,π⁰}	0 ⁺ → (K _S ⁰ K _S ⁰) _{ρ±,ρ∓,π⁰}	0 ⁺ → (K _S ⁰ K _S ⁰) _{ρ±,ρ∓,π⁰}	0 ⁺ → (K _S ⁰ K _S ⁰) _{ρ±,ρ∓,π⁰}	0 ⁺ → (K _S ⁰ K _S ⁰) _{ρ±,ρ∓,π⁰}	0 ⁺ → (K _S ⁰ K _S ⁰) _{ρ±,ρ∓,π⁰}	0 ⁺ → (K _S ⁰ K _S ⁰) _{ρ±,ρ∓,π⁰}	0 ⁺ → (K _S ⁰ K _S ⁰) _{ρ±,ρ∓,π⁰}	0 ⁺ → (K _S ⁰ K _S ⁰) _{ρ±,ρ∓,π⁰}	0 ⁺ → (K _S ⁰ K _S ⁰) _{ρ±,ρ∓,π⁰}	0 ⁺ → (K _S ⁰ K _S ⁰) _{ρ±,ρ∓,π⁰}
1 ⁺⁺ → K ⁺ (892) ⁰ K _S ⁰	1 ⁺⁺ → K ⁺ (892) ⁰ K _S ⁰	1 ⁺⁺ → K ⁺ (892) ⁰ K _S ⁰	1 ⁺⁺ → K ⁺ (892) ⁰ K _S ⁰	1 ⁺⁺ → K ⁺ (892) ⁰ K _S ⁰	1 ⁺⁺ → K ⁺ (892) ⁰ K _S ⁰	1 ⁺⁺ → K ⁺ (892) ⁰ K _S ⁰	1 ⁺⁺ → K ⁺ (892) ⁰ K _S ⁰	1 ⁺⁺ → K ⁺ (892) ⁰ K _S ⁰	1 ⁺⁺ → K ⁺ (892) ⁰ K _S ⁰	1 ⁺⁺ → K ⁺ (892) ⁰ K _S ⁰	1 ⁺⁺ → K ⁺ (892) ⁰ K _S ⁰

Table 2. The fit components of the nominal solutions for 24 bins of 15 MeV/c² width in the K_S⁰K_S⁰π⁰ invariant mass spectrum.

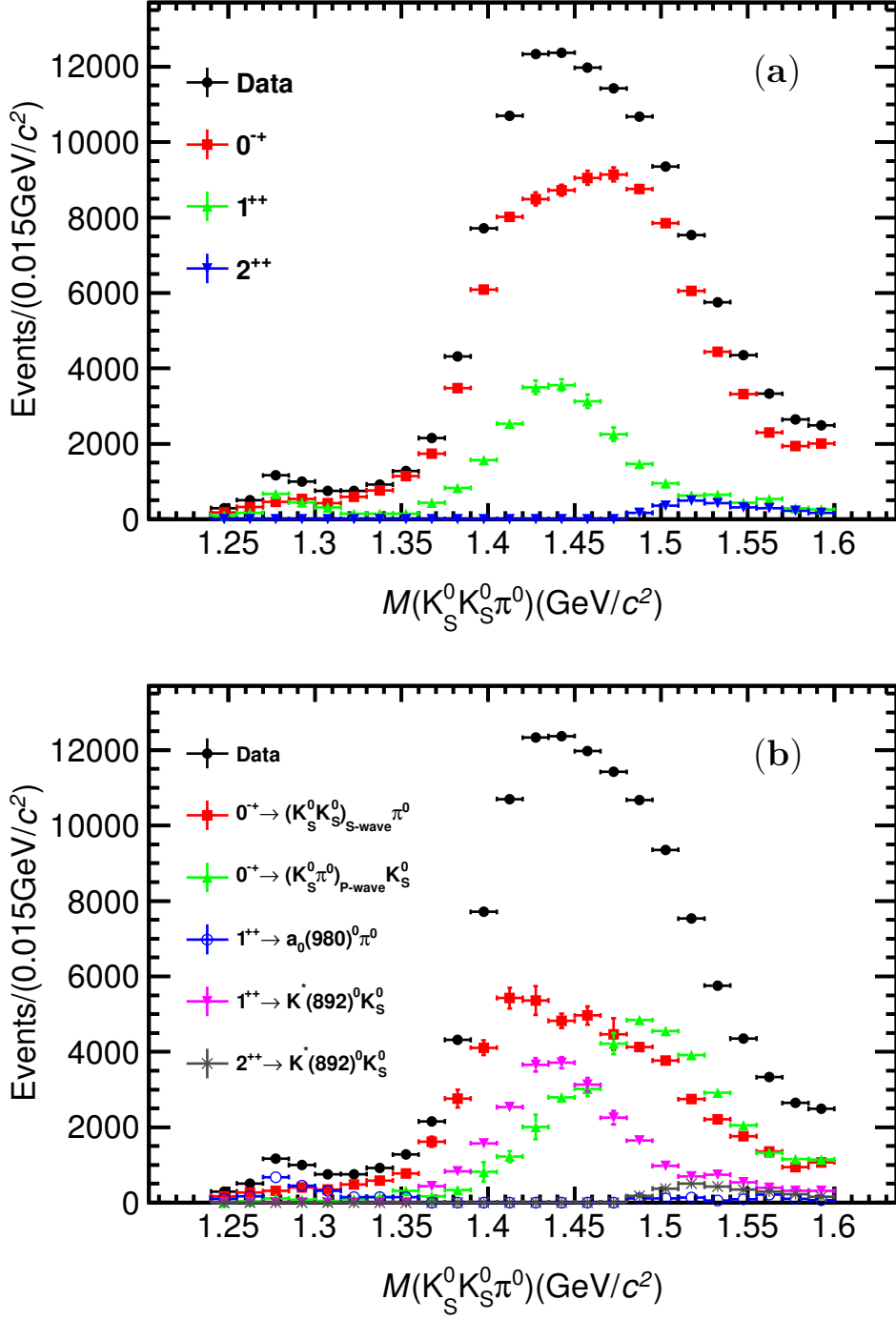


Figure 3. The $K_S^0 K_S^0 \pi^0$ intensity spectra for the (a) dominant spin-parity components and (b) dominant decay modes for different spin-parity components obtained from the MI PWA results. The uncertainty on the total data is statistical, and the uncertainties on the others are obtained from the PWA in each bin.

4.3 Mass dependent PWA

A mass dependent (MD) PWA is also performed. All possible intermediate states listed in the PDG [12] with mass less than $1.6 \text{ GeV}/c^2$, and satisfying spin-parity, charge conjugation and isospin conservation, e.g., the $\eta(1295)$, $\eta(1405)$, $\eta(1475)$, $f_1(1285)$, $f_1(1420)$, $f_1(1510)$, $f_2(1270)$, $f_2(1525)$ and $f_2(1565)$, are considered as candidates in the analysis. Additionally, non-resonant processes with different spin-parities are also taken into consideration when searching for the nominal solution. These kinds of non-resonant components can mimic the contributions of the tails from higher mass resonances with different spin-parities and decay modes as well. The masses and widths of intermediate states from J/ψ radiative decay are floating in the fit, while those of the resonances decaying into $K_S^0 K_S^0$ or $K_S^0 \pi^0$ final states are fixed to the PDG values [12] or published results [49] as done in the MI PWA. All possible intermediate states and decay modes are tried in the fits, and only those with significance larger than 5σ are retained.

Finally, the nominal solution includes two pseudoscalar states, the $\eta(1405)$ and $\eta(1475)$, two axial vector states, the $f_1(1285)$ and $f_1(1420)$ and a tensor state, the $f_2(1525)$. In total, 14 components are considered, and the fractions of the various components, as well as the interference fractions between any two components are presented in table 3. The calculation of the fractions for individual components involves the PHSP MC truth information without detector acceptance or resolution effects. The fraction for the i^{th} component is defined as:

$$F_i = \frac{\sum_{k=1}^{N_{\text{truth}}} |A_i|_k^2}{\sum_{k=1}^{N_{\text{truth}}} |A|_k^2}, \quad (4.14)$$

and the interference between the i^{th} and j^{th} components is defined as (where $I_{ij} = I_{ji}$):

$$I_{ij} = \frac{\sum_{k=1}^{N_{\text{truth}}} 2\text{Re}[A_i A_j^*]_k}{\sum_{k=1}^{N_{\text{truth}}} |A|_k^2}, \quad (4.15)$$

where N_{truth} is the number of PHSP MC events at the generator level; A_i and A_j are the amplitudes corresponding to the i^{th} and j^{th} components in the MD PWA nominal solution as defined in eq. (4.1), respectively; $A = \sum_i A_i$ is the total amplitude describing the decay processes from the J/ψ to the final state $\gamma K_S^0 K_S^0 \pi^0$ in the MD PWA nominal solution. These fractions will not sum to unity if there is net constructive or destructive interference. In order to determine the statistical uncertainties of the fractions, the amplitude coefficients are randomly sampled by a Gaussian-distributed amount set by the covariance matrix. Then the distribution of each fraction is fitted with a Gaussian function and the width of the Gaussian function is defined as the uncertainty of the fraction. The optimized masses and widths of the intermediate states, product branching fractions of $J/\psi \rightarrow \gamma R_1$ with $R_1 \rightarrow K_S^0 R_2 \rightarrow K_S^0 K_S^0 \pi^0$ or $R_1 \rightarrow \pi^0 R_2 \rightarrow K_S^0 K_S^0 \pi^0$, the statistical significances of the predominant components are calculated accordingly and summarized in table 4, where the first uncertainties are statistical and the second are systematic.

Figures 4(a)-(c) show distributions of the data and the MD PWA fit projections (PHSP MC sample weighted with the differential cross sections) on the invariant mass of $K_S^0 K_S^0 \pi^0$, $K_S^0 K_S^0$ and $K_S^0 \pi^0$, individually, while figures 4(d)-(g) show various angular distributions.

Components	(1)	(2)	(3)	(4)	(5)	(6)	(7)	(8)	(9)	(10)	(11)	(12)	(13)	(14)
(1). $J/\psi \rightarrow \gamma \text{PHSP}(0^{-+}) \rightarrow \gamma K^{*}(892)^0 K_S^0 \pi^0 \rightarrow \gamma K_S^0 K_S^0 \pi^0$	3.4 ± 0.1	0.9 ± 0.1	9.0 ± 0.1	-2.7 ± 0.1	-1.2 ± 0.1	0.0 ± 0.0	0.3 ± 0.1	0.0 ± 0.0	1.4 ± 0.1	1.4 ± 0.1	0.0 ± 0.0	0.0 ± 0.0	0.2 ± 0.1	0.0 ± 0.0
(2). $J/\psi \rightarrow \gamma \text{PHSP}(1^{++}) \rightarrow \gamma K^{*}(892)^0 K_S^0 \pi^0 \rightarrow \gamma K_S^0 K_S^0 \pi^0$	2.9 ± 0.1	1.2 ± 0.1	1.2 ± 0.1	0.3 ± 0.1	-1.0 ± 0.2	0.0 ± 0.0	0.0 ± 0.0	0.0 ± 0.0	0.2 ± 0.1	0.4 ± 0.1	1.4 ± 0.1	1.0 ± 0.2	0.0 ± 0.1	0.0 ± 0.0
(3). $J/\psi \rightarrow \gamma \eta(1405) \rightarrow \gamma K_S^0(K_S^0 \pi^0)_{P\text{-wave}} \rightarrow \gamma K_S^0 K_S^0 \pi^0$	9.5 ± 0.2	1.2 ± 0.1	9.5 ± 0.2	-1.0 ± 0.1	-1.6 ± 0.1	0.0 ± 0.0	-1.7 ± 0.1	0.0 ± 0.1	1.1 ± 0.1	2.4 ± 0.1	0.0 ± 0.0	0.0 ± 0.1	1.0 ± 0.1	0.0 ± 0.0
(4). $J/\psi \rightarrow \gamma \eta(1475) \rightarrow \gamma K_S^0(K_S^0 \pi^0)_{P\text{-wave}} \rightarrow \gamma K_S^0 K_S^0 \pi^0$	11.2 ± 0.2	2.0 ± 0.1	11.2 ± 0.2	-1.0 ± 0.1	2.0 ± 0.1	0.0 ± 0.0	-2.0 ± 0.1	0.0 ± 0.0	-1.9 ± 0.1	-1.0 ± 0.1	0.0 ± 0.0	0.0 ± 0.0	-0.8 ± 0.1	0.3 ± 0.1
(5). $J/\psi \rightarrow \gamma f_1(1420) \rightarrow \gamma K^{*}(892)^0 K_S^0 \pi^0 \rightarrow \gamma K_S^0 K_S^0 \pi^0$	18.9 ± 0.3	-0.1 ± 0.1	18.9 ± 0.3	-0.1 ± 0.1	18.9 ± 0.3	2.2 ± 0.1	-0.7 ± 0.1	0.0 ± 0.1	0.0 ± 0.1	0.0 ± 0.0	0.0 ± 0.2	0.0 ± 0.1	-5.8 ± 0.3	-0.2 ± 0.1
(6). $J/\psi \rightarrow \gamma f_2(1525) \rightarrow \gamma K^{*}(892)^0 K_S^0 \pi^0 \rightarrow \gamma K_S^0 K_S^0 \pi^0$														
(7). $J/\psi \rightarrow \gamma \text{PHSP}(0^{-+}) \rightarrow \gamma a_0(980)^0 \pi^0 \rightarrow \gamma K_S^0 K_S^0 \pi^0$														
(8). $J/\psi \rightarrow \gamma \text{PHSP}(2^{-+}) \rightarrow \gamma a_0(980)^0 \pi^0 \rightarrow \gamma K_S^0 K_S^0 \pi^0$														
(9). $J/\psi \rightarrow \gamma \eta(1405) \rightarrow \gamma(K_S^0 K_S^0)_{S\text{-wave}} \pi^0 \rightarrow \gamma K_S^0 K_S^0 \pi^0$														
(10). $J/\psi \rightarrow \gamma \eta(1475) \rightarrow \gamma(K_S^0 K_S^0)_{S\text{-wave}} \pi^0 \rightarrow \gamma K_S^0 K_S^0 \pi^0$														
(11). $J/\psi \rightarrow \gamma f_1(1285) \rightarrow \gamma a_0(980)^0 \pi^0 \rightarrow \gamma K_S^0 K_S^0 \pi^0$														
(12). $J/\psi \rightarrow \gamma f_1(1420) \rightarrow \gamma a_0(980)^0 \pi^0 \rightarrow \gamma K_S^0 K_S^0 \pi^0$														
(13). $J/\psi \rightarrow \gamma \eta(1405) \rightarrow \gamma a_2(1320)^0 \pi^0 \rightarrow \gamma K_S^0 K_S^0 \pi^0$														
(14). $J/\psi \rightarrow \gamma \eta(1475) \rightarrow \gamma a_2(1320)^0 \pi^0 \rightarrow \gamma K_S^0 K_S^0 \pi^0$														

Table 3. Fraction of each component and interference fractions between two components (%) in the MD PWA nominal solution. The uncertainties are statistical only.

Resonance	$M(\text{MeV}/c^2)$	$\Gamma(\text{MeV})$	Decay Mode	B.F.	Sig. (σ)
$\eta(1405)$	$1391.7 \pm 0.7_{-0.3}^{+11.3}$	$60.8 \pm 1.2_{-12.0}^{+5.5}$	$J/\psi \rightarrow \gamma \eta(1405) \rightarrow \gamma K_S^0(K_S^0 \pi^0)_{\text{P-wave}} \rightarrow \gamma K_S^0 K_S^0 \pi^0$	$(5.84 \pm 0.12_{-3.36}^{+2.03}) \times 10^{-5}$	$\gg 35$
			$J/\psi \rightarrow \gamma \eta(1405) \rightarrow \gamma (K_S^0 K_S^0)_{\text{S-wave}} \pi^0 \rightarrow \gamma K_S^0 K_S^0 \pi^0$	$(2.88 \pm 0.04_{-0.38}^{+1.64}) \times 10^{-5}$	18.4
$\eta(1475)$	$1507.6 \pm 1.6_{-32.2}^{+15.5}$	$115.8 \pm 2.4_{-10.9}^{+14.8}$	$J/\psi \rightarrow \gamma \eta(1475) \rightarrow \gamma K_S^0(K_S^0 \pi^0)_{\text{P-wave}} \rightarrow \gamma K_S^0 K_S^0 \pi^0$	$(6.58 \pm 0.12_{-2.82}^{+3.98}) \times 10^{-5}$	$\gg 35$
			$J/\psi \rightarrow \gamma \eta(1475) \rightarrow \gamma (K_S^0 K_S^0)_{\text{S-wave}} \pi^0 \rightarrow \gamma K_S^0 K_S^0 \pi^0$	$(3.99 \pm 0.09_{-0.66}^{+0.41}) \times 10^{-5}$	$\gg 35$
$f_1(1285)$	$1280.2 \pm 0.6_{-1.5}^{+1.2}$	$28.2 \pm 1.1_{-2.9}^{+5.5}$	$J/\psi \rightarrow \gamma f_1(1285) \rightarrow \gamma a_0(980)^0 \pi^0 \rightarrow \gamma K_S^0 K_S^0 \pi^0$	$(8.55 \pm 0.41_{-1.04}^{+3.42}) \times 10^{-6}$	$\gg 35$
$f_1(1420)$	$1433.5 \pm 1.1_{-0.7}^{+27.9}$	$95.9 \pm 2.3_{-10.9}^{+13.6}$	$J/\psi \rightarrow \gamma f_1(1420) \rightarrow \gamma K^*(892)^0 K_S^0 \rightarrow \gamma K_S^0 K_S^0 \pi^0$	$(7.25 \pm 0.12_{-1.25}^{+0.73}) \times 10^{-5}$	$\gg 35$
			$J/\psi \rightarrow \gamma f_1(1420) \rightarrow \gamma a_0(980)^0 \pi^0 \rightarrow \gamma K_S^0 K_S^0 \pi^0$	$(4.62 \pm 0.36_{-1.94}^{+2.36}) \times 10^{-6}$	17.8
$f_2(1525)$	$1515.4 \pm 2.5_{-7.6}^{+3.2}$	$64.0 \pm 4.3_{-6.1}^{+2.0}$	$J/\psi \rightarrow \gamma f_2(1525) \rightarrow \gamma K^*(892)^0 K_S^0 \rightarrow \gamma K_S^0 K_S^0 \pi^0$	$(9.47 \pm 0.43_{-0.66}^{+1.51}) \times 10^{-6}$	23.8

Table 4. Masses (M), widths (Γ), branching fractions (B.F.) and significances (Sig.) of predominant components in the MD PWA nominal solution. The first uncertainties are statistical and the second ones are systematic.

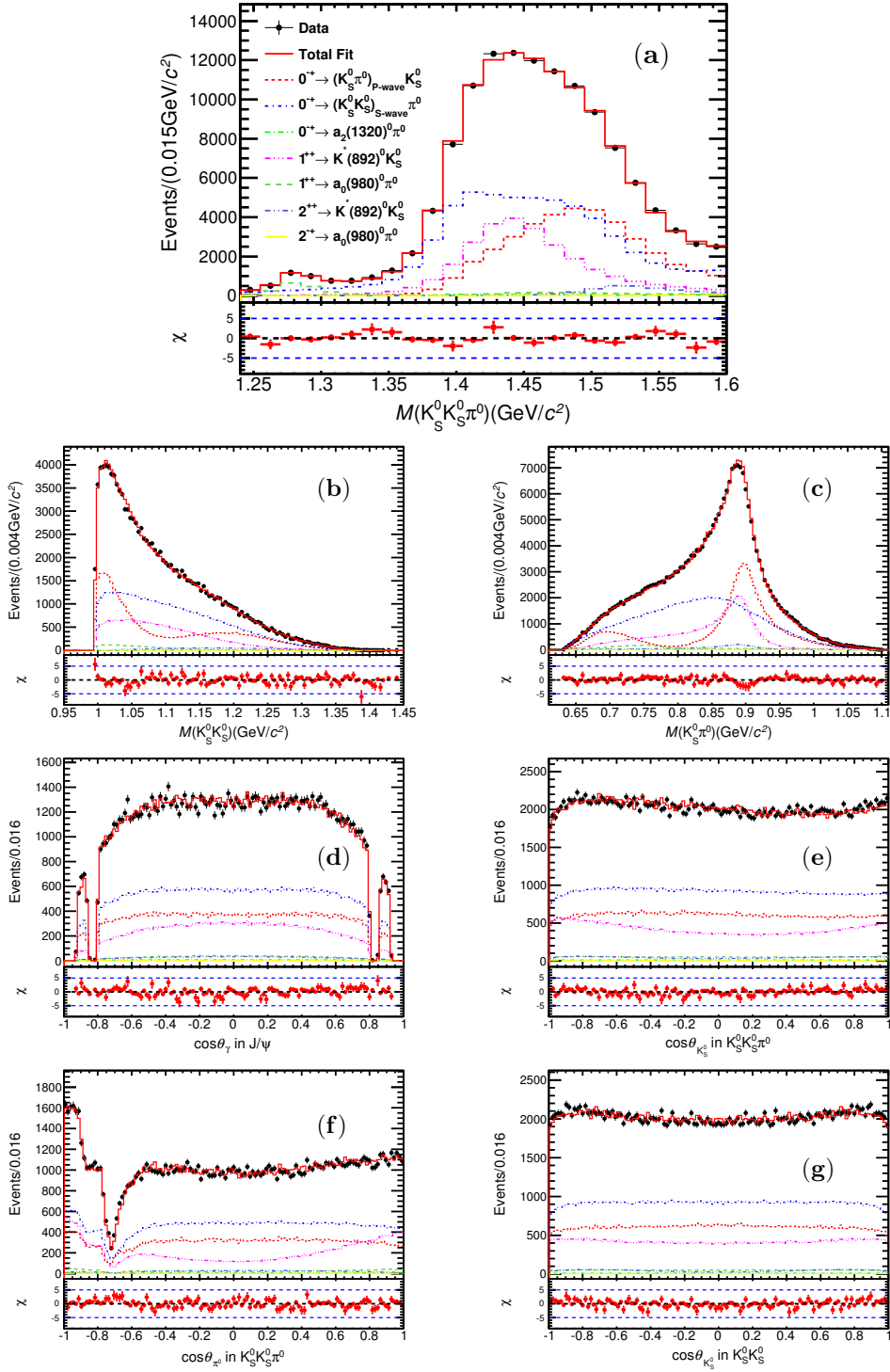


Figure 4. Superposition of data and the MD PWA fit projections for invariant mass distributions of (a) $K_S^0 K_S^0 \pi^0$, (b) $K_S^0 K_S^0$, and (c) $K_S^0 \pi^0$. The $\cos \theta$ distributions of (d) γ in J/ψ helicity frame, (e) K_S^0 and (f) π^0 in $K_S^0 K_S^0 \pi^0$ system helicity frame, (g) K_S^0 in $K_S^0 K_S^0 \pi^0$ system helicity frame. The pull projection of residual is shown beneath each distribution correspondingly.

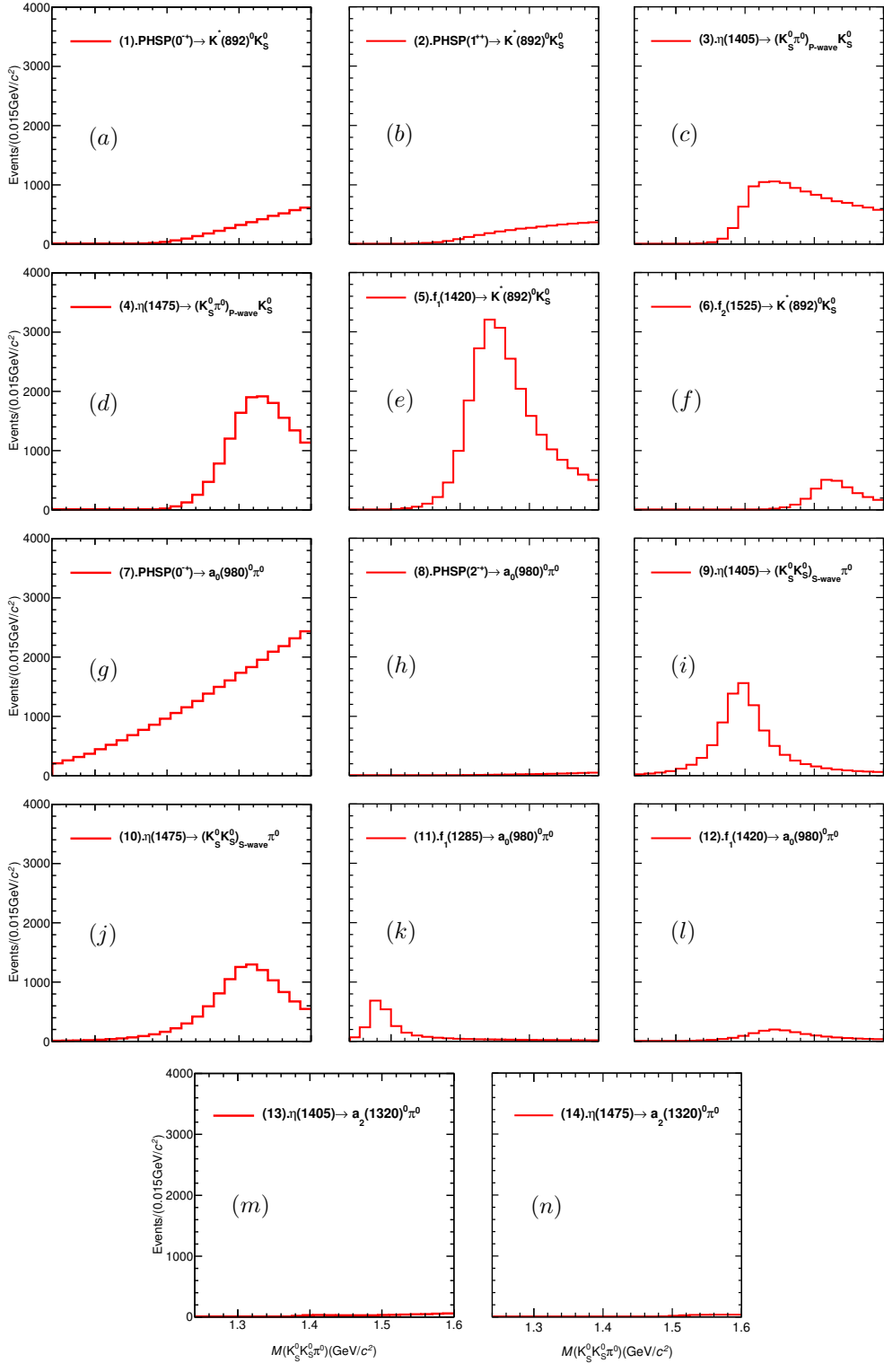


Figure 5. Invariant mass distribution of $K_S^0 K_S^0 \pi^0$ for each of the 14 individual components corresponding to table 3 included in the MD PWA nominal solution.

As a supplement for figure 4(a) in detail, the figure 5 shows the $M(K_S^0 K_S^0 \pi^0)$ spectrum for each of the 14 individual components corresponding to table 3 included in the MD PWA nominal solution. Additionally, the dips on the $\cos\theta$ distribution of γ in J/ψ helicity frame shown in figure 4(d) are caused by the acceptance of the EMC detector, and the dips on $\cos\theta$ distribution of π^0 in $K_S^0 K_S^0 \pi^0$ helicity frame shown in figure 4(f) are correlated with the veto of ω on the $\gamma\pi^0$ invariant mass spectrum which is applied on the event selection part. The pull projection of residual beneath each distribution is displayed to demonstrate the comparison between data and MC projection correspondingly, where the χ is defined as

$$\chi = \frac{n_i - \nu_i}{\sqrt{\nu_i}}, \quad (4.16)$$

where n_i and ν_i are the number of entries for the data and the fit projections of the nominal solution in the i^{th} bin, respectively.

To validate the consistency between the MI and MD PWA results, comparisons of the $K_S^0 K_S^0 \pi^0$ intensity spectra for individual spin-parity components obtained by the two PWA approaches are shown in figure 6(a), where good agreement is observed. We also compare the distributions of the pseudoscalar component decaying into $(K_S^0 K_S^0)_{\text{S-wave}} \pi^0$, $(K_S^0 \pi^0)_{\text{P-wave}} K_S^0$ and the axial vector component decaying into $a_0(980)^0 \pi^0$, $K^*(892)^0 K_S^0$ between the two approaches, individually, as shown in figures 6(b) and (c), where good agreement is also achieved.

As described previously, the lineshape and dynamics of the pseudoscalar component are of great interest in this analysis. Therefore, different scenarios are tried in the MD analysis. An alternative fit is performed by replacing the two pseudoscalar states $\eta(1405)$ and $\eta(1475)$ with one resonance with floating resonance parameters. The result shows the NLL value is worsen by 1564.4. The result from the TSM test by considering both $\eta(1440)$ and $f_1(1420)$ TSM contributions in the MD PWA, where the intermediate on-shell $K^* K + c.c$ can exchange an on-shell kaon or anti-kaon and then rescatter to $a_0(980)^0 \pi^0$ in this process [28, 29], shows the NLL value is worse by 1169.4. The description of the $K_S^0 K_S^0 \pi^0$ invariant mass spectrum deteriorates significantly compared with the two states scenario.

5 Systematic uncertainties

In the MD PWA, the sources of systematic uncertainties can be classified into two categories, i.e., those associated with event reconstruction and selection, and those related to the PWA.

The systematic uncertainties associated with the event reconstruction and selection are applied in the branching fraction measurement only, and mainly include those from the photon detection efficiency, K_S^0 reconstruction efficiency, kinematic fit, the number of J/ψ events, and the branching fractions of $K_S^0 \rightarrow \pi^+ \pi^-$ and $\pi^0 \rightarrow \gamma\gamma$. The systematic uncertainty of the photon detection efficiency is 1.0% per photon, obtained by studying the control sample of $J/\psi \rightarrow \rho\pi$ [53]. Therefore, 3% is assigned as the corresponding uncertainty for three photons. The systematic uncertainty of K_S^0 reconstruction efficiency is studied with the control samples of $J/\psi \rightarrow K^{*\pm} K^{*\mp}$ and $J/\psi \rightarrow \phi K_S^0 K^\pm \pi^\mp$, and is 1%

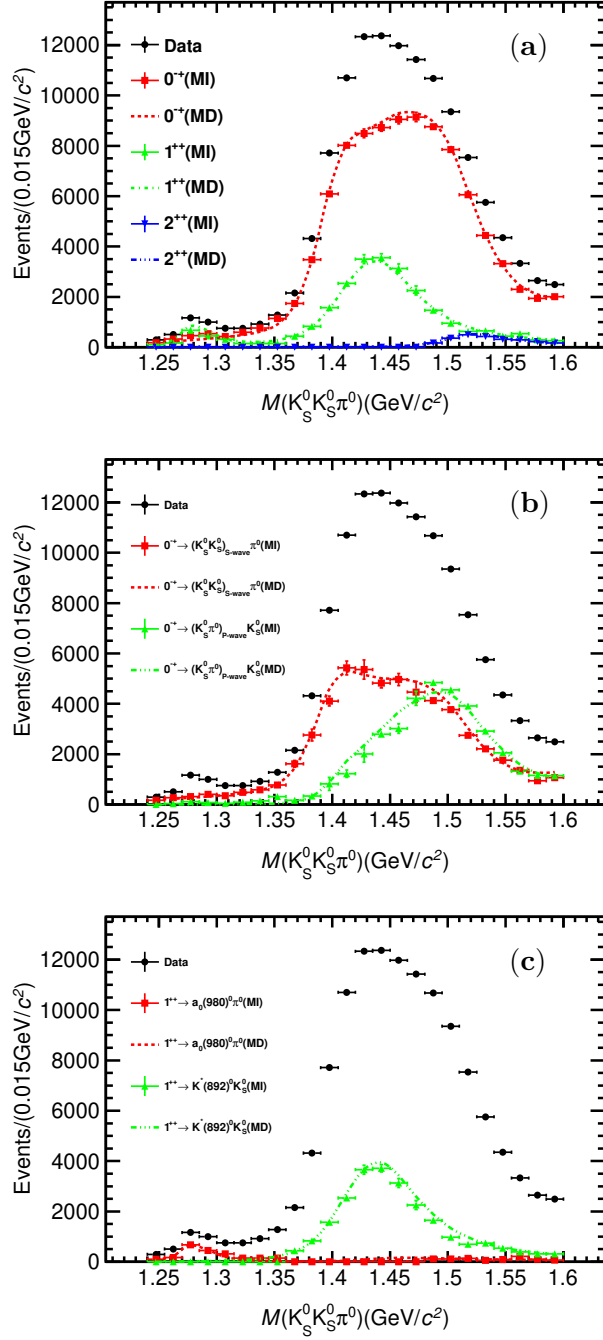


Figure 6. The $K_S^0 K_S^0 \pi^0$ intensity spectra for the (a) dominant spin-parity components, (b) dominant decay modes for the pseudoscalar component, and (c) dominant decay modes for the axial vector component. The dots with error bars and the dotted lines are the intensity obtained from the MI PWA and MD PWA results, respectively. The uncertainty on the total data is statistical, and those of the others are obtained from the PWA in each bin.

Source	Uncertainty(%)
Photon detection	3.0
K_S^0 reconstruction	2.0
Kinematic fit	1.6
Number of J/ψ events	0.4
Intermediate branching fractions	0.2
Total	4.0

Table 5. Summary of systematic uncertainties related to event selection for the determination of the branching fraction (relative uncertainties).

Source	$\eta(1405)$		$\eta(1475)$		$f_1(1285)$		$f_1(1420)$		$f_2(1525)$	
	ΔM	$\Delta\Gamma$	ΔM	$\Delta\Gamma$	ΔM	$\Delta\Gamma$	ΔM	$\Delta\Gamma$	ΔM	$\Delta\Gamma$
Breit-Wigner formula	+11.0	+5.2 -11.8	+15.5 -31.6	+14.6	+0.8 -1.5	+0.6 -2.9	+27.9 -0.5	+13.3 -9.9	+2.6 -7.5	+2.0 -5.1
Resonance parameters	+2.5	+1.8	-5.6	-10.8	+0.3	+1.8	-0.2	-2.4	+1.6	-3.0
Extra components	+0.1 -0.3	+0.6 -2.0	+0.1 -2.2	+2.3 -1.8	+0.8 -0.2	+5.2 -0.1	+1.5 -0.5	+2.7 -3.9	+1.1	-1.4
Total	+11.3 -0.3	+5.5 -12.0	+15.5 -32.2	+14.8 -10.9	+1.2 -1.5	+5.5 -2.9	+27.9 -0.7	+13.6 -10.9	+3.2 -7.5	+2.0 -6.1

Table 6. Summary of the systematic uncertainty sources and their corresponding contributions to the systematic uncertainties in masses (MeV/c^2) and widths (MeV) of $\eta(1405)$, $\eta(1475)$, $f_1(1285)$, $f_1(1420)$ and $f_2(1525)$, denoted as ΔM and $\Delta\Gamma$, respectively.

per K_S^0 candidate [54]. Therefore, 2% is assigned as the corresponding uncertainty for the two K_S^0 candidates. The systematic uncertainty associated with the kinematic fit is 1.6%, obtained by the track helix parameter correction method [55]. The total number of J/ψ decays is obtained using inclusive hadron events, and the uncertainty is 0.4% [30]. The uncertainties associated with the decay branching fractions of $K_S^0 \rightarrow \pi^+\pi^-$ and $\pi^0 \rightarrow \gamma\gamma$ are quoted from the PDG [12]. All the uncertainties associated with event reconstruction and selection are summarized in table 5, and the total uncertainty is 4%, which is the quadrature sum of the individual values.

The systematic uncertainties associated with the PWA, which are applied in both measurements of branching fractions and the resonance parameters in the MD approach, include:

- *Uncertainty from the resonance parametrization form.* In the nominal fit, the intermediate states are parameterized by a relativistic BW function with a constant width. Since the $\eta(1405)$, $\eta(1475)$ and $f_1(1420)$ are close to the threshold of $K^*(892)K$, an alternative BW function with mass-dependent width is used to parameterize the resonances,

$$BW(s) = \frac{1}{M^2 - s - iM\Gamma(s)}, \quad (5.1)$$

Resonance	Decay Mode	Event selection	Breit-Wigner formula	Resonance parameters	Extra components	Total
$\eta(1405)$	$J/\psi \rightarrow \gamma\eta(1405) \rightarrow \gamma K_S^0(K_S^0\pi^0)_{P\text{-wave}} \rightarrow \gamma K_S^0 K_S^0\pi^0$	± 4.0	$+28.1$ -56.8	$+20.0$	$+2.8$ -7.8	$+34.8$ -57.5
	$J/\psi \rightarrow \gamma\eta(1405) \rightarrow \gamma(K_S^0 K_S^0)_{S\text{-wave}}\pi^0 \rightarrow \gamma K_S^0 K_S^0\pi^0$	± 4.0	$+19.0$ -7.5	$+53.1$	$+6.1$ -10.0	$+56.9$ -13.1
$\eta(1475)$	$J/\psi \rightarrow \gamma\eta(1475) \rightarrow \gamma K_S^0(K_S^0\pi^0)_{P\text{-wave}} \rightarrow \gamma K_S^0 K_S^0\pi^0$	± 4.0	$+59.4$ -42.5	$+8.9$	$+5.8$ -3.1	$+60.5$ -42.8
	$J/\psi \rightarrow \gamma\eta(1475) \rightarrow \gamma(K_S^0 K_S^0)_{S\text{-wave}}\pi^0 \rightarrow \gamma K_S^0 K_S^0\pi^0$	± 4.0	$+5.5$ -7.4	-13.7	$+7.8$ -4.3	$+10.3$ -16.6
$f_1(1285)$	$J/\psi \rightarrow \gamma f_1(1285) \rightarrow \gamma a_0(980)^0\pi^0 \rightarrow \gamma K_S^0 K_S^0\pi^0$	± 4.0	$+1.0$ -11.2	$+4.3$	$+30.6$ -2.5	$+40.0$ -12.2
$f_1(1420)$	$J/\psi \rightarrow \gamma f_1(1420) \rightarrow \gamma K^{*}(892)^0 K_S^0 \rightarrow \gamma K_S^0 K_S^0\pi^0$	± 4.0	$+2.5$ -16.8	$+6.4$	$+6.1$ -1.2	$+10.0$ -17.3
	$J/\psi \rightarrow \gamma f_1(1420) \rightarrow \gamma a_0(980)^0\pi^0 \rightarrow \gamma K_S^0 K_S^0\pi^0$	± 4.0	$+15.8$ -41.8	$+7.8$	$+47.8$	$+51.1$ -42.0
$f_2(1525)$	$J/\psi \rightarrow \gamma f_2(1525) \rightarrow \gamma K^{*}(892)^0 K_S^0 \rightarrow \gamma K_S^0 K_S^0\pi^0$	± 4.0	$+15.3$ -4.7	-3.3	$+1.9$ -0.5	$+15.9$ -7.0

Table 7. Summary of the systematic error sources and their corresponding contributions to the branching fractions (relative uncertainties, in %).

with

$$\Gamma(s) = \Gamma(M^2) \left(\frac{M}{\sqrt{s}} \right) \left(\frac{\rho(s)}{\rho(M^2)} \right)^{2l+1} B_l^2(\rho(s)), \quad (5.2)$$

where s is the invariant mass squared of the intermediate states, M and $\Gamma(M^2)$ are the corresponding nominal mass and width, ρ is the momentum of the daughter particle in its mother resonance rest frame calculated by the invariant mass squared of the mother resonance, $B_l(\rho(s))$ is the Blatt-Weisskopf barrier factor [56] and l is the orbital angular momentum.

- *Uncertainty from resonance parameters.* In the nominal fit, the resonant parameters of $a_0(980)^0$, $K^*(892)^0$ and $a_2(1320)^0$ states are fixed. The related uncertainties are evaluated with alternative fits in which these resonance parameters are varied within one standard deviation of the PDG values [12] or published results [49].
- *Uncertainty from extra components.* Uncertainties from possible extra components are estimated by adding the processes $f_1(1510) \rightarrow K^*(892)^0 K_S^0$, $\eta(1295) \rightarrow a_0(980)^0 \pi^0$, $f_1(1420) \rightarrow (K_S^0 \pi^0)_{\text{P-phsp}} K_S^0$ and $f_1(1285) \rightarrow (K_S^0 \pi^0)_{\text{P-phsp}} K_S^0$, which are the four most significant extra components evaluated from data, into the nominal configuration individually.

For each alternative fit performed to estimate the systematic uncertainties from the PWA fit procedure, the changes of the measurements are taken as the one-sided systematic uncertainties. For each measurement, the individual uncertainties are assumed to be independent and are added in quadrature to obtain the total systematic uncertainty on the negative and positive sides, respectively. The sources of systematic uncertainties are applied to the measurements of masses and widths of intermediate states, and their contributions are summarized in table 6. The relative systematic uncertainties relevant to the branching fraction measurements are summarized in table 7.

6 Summary

In summary, mass independent and dependent PWAs have been performed on the decay $J/\psi \rightarrow \gamma K_S^0 K_S^0 \pi^0$ with $M(K_S^0 K_S^0 \pi^0) < 1.6 \text{ GeV}/c^2$ based on 10.09×10^9 J/ψ decays collected with the BESIII detector. The analyses show good consistency with each other in the intensity of individual components, and exhibit that the pseudoscalar and axial vector components are the dominant contributions. The mass dependent PWA shows that the pseudoscalar component can be well described with the two isoscalar states using relativistic Breit-Wigner model, i.e., $\eta(1405)$ with a mass of $1391.7 \pm 0.7_{-0.3}^{+11.3} \text{ MeV}/c^2$ and a width of $60.8 \pm 1.2_{-12.0}^{+5.5} \text{ MeV}$ and $\eta(1475)$ with a mass of $1507.6 \pm 1.6_{-32.2}^{+15.5} \text{ MeV}/c^2$ and a width of $115.8 \pm 2.4_{-11.0}^{+14.8} \text{ MeV}$, and both decay into $(K_S^0 K_S^0)_{\text{S-wave}} \pi^0$ and $(K_S^0 \pi^0)_{\text{P-wave}} K_S^0$. The axial vector component can be well described with $f_1(1285) \rightarrow a_0(980)^0 \pi^0$, $f_1(1420) \rightarrow a_0(980)^0 \pi^0$ and $f_1(1420) \rightarrow K^*(892)^0 K_S^0$. The tensor component $f_2(1525) \rightarrow K^*(892)^0 K_S^0$ is observed for the first time in this process.

For the pseudoscalar component, the relatively flat lineshape between $1.4 \text{ GeV}/c^2$ and $1.5 \text{ GeV}/c^2$ rules out one standard resonance parameterization. In addition, the current TSM models [26–29] can not describe data well. This analysis provides a precision measurement of the pseudoscalar component, and is essential to study the dynamics of pseudoscalar structure in this mass region. More studies on the TSM and other phenomenological mechanisms are necessary to improve our understanding of the isoscalar pseudoscalar spectrum.

Acknowledgments

The BESIII collaboration thanks the staff of BEPCII and the IHEP computing center for their strong support. This work is supported in part by National Key R&D Program of China under Contracts Nos. 2020YFA0406300, 2020YFA0406400; National Natural Science Foundation of China (NSFC) under Contracts Nos. 11335008, 11625523, 11635010, 11705192, 11735014, 11835012, 11922511, 11935015, 11935016, 11935018, 11950410506, 11961141012, 12022510, 12025502, 12035009, 12035013, 12061131003, 12105276, 12122509, 12192260, 12192261, 12192262, 12192263, 12192264, 12192265, 12235017; the Chinese Academy of Sciences (CAS) Large-Scale Scientific Facility Program; Joint Large-Scale Scientific Facility Funds of the NSFC and CAS under Contract No. U1732263, U1832103, U1832207, U2032111; the CAS Center for Excellence in Particle Physics (CCEPP); 100 Talents Program of CAS; The Institute of Nuclear and Particle Physics (INPAC) and Shanghai Key Laboratory for Particle Physics and Cosmology; ERC under Contract No. 758462; European Union’s Horizon 2020 research and innovation programme under Marie Skłodowska-Curie grant agreement under Contract No. 894790; German Research Foundation DFG under Contracts Nos. 443159800, Collaborative Research Center CRC 1044, GRK 2149; Istituto Nazionale di Fisica Nucleare, Italy; Ministry of Development of Turkey under Contract No. DPT2006K-120470; National Science and Technology fund; National Science Research and Innovation Fund (NSRF) via the Program Management Unit for Human Resources & Institutional Development, Research and Innovation under Contract No. B16F640076; STFC (United Kingdom); Suranaree University of Technology (SUT), Thailand Science Research and Innovation (TSRI), and National Science Research and Innovation Fund (NSRF) under Contract No. 160355; The Royal Society, U.K. under Contracts Nos. DH140054, DH160214; The Swedish Research Council; U.S. Department of Energy under Contract No. DE-FG02-05ER41374

A Formulas of covariant tensor amplitudes

As a supplement, we provide the formulas of covariant tensor amplitudes applied in PWA nominal solution referring to ref. [47], where K_S^0, K_S^0, π^0 are denoted as particle 1, 2, 3. The corresponding intermediate resonances and decay modes are listed in the table 3.

For the $J/\psi \rightarrow \gamma 0^{-+}$ vertex, there is one independent coupling:

$$\langle \gamma 0^{-+} | (K^* K) 1 \rangle = S_{\mu\nu} B_1(Q_{\psi\gamma X}) f_{(123)}^{(0^{-+})} \left[\tilde{t}_{(K^*K)\lambda}^{(1)} \tilde{t}_{(13)}^{(1)\lambda} f_{(13)}^{(K^*)} + \tilde{t}_{(K^*K)\lambda}^{(1)} \tilde{t}_{(23)}^{(1)\lambda} f_{(23)}^{(K^*)} \right] \quad (\text{A.1})$$

$$\langle \gamma 0^{-+} | (a_0 \pi^0) 1 \rangle = S_{\mu\nu} B_1(Q_{\psi\gamma X}) f_{(123)}^{(0^{-+})} f_{(12)}^{(a_0)} \quad (\text{A.2})$$

$$\langle \gamma 0^{-+} | (a_2 \pi^0) 1 \rangle = S_{\mu\nu} B_1(Q_{\psi\gamma X}) f_{(123)}^{(0^{-+})} f_{(12)}^{(a_2)} \tilde{t}_{(a_2\pi^0)\gamma\delta}^{(2)} \tilde{t}_{(12)}^{(2)\gamma\delta} \quad (\text{A.3})$$

For the $J/\psi \rightarrow \gamma 1^{++}$ vertex, there are two independent couplings:

$$\langle \gamma 1^{++} | (K^* K) 1 \rangle = \epsilon_{\mu\nu\alpha\beta} p_\psi^\alpha f_{(123)}^{(1^{++})} \left[\tilde{t}_{(13)}^{(1)\beta} f_{(13)}^{(K^*)} + \tilde{t}_{(23)}^{(1)\beta} f_{(23)}^{(K^*)} \right] \quad (\text{A.4})$$

$$\langle \gamma 1^{++} | (K^* K) 2 \rangle = q_\mu S_{\nu\beta} B_2(Q_{\psi\gamma X}) f_{(123)}^{(1^{++})} \left[\tilde{t}_{(13)}^{(1)\beta} f_{(13)}^{(K^*)} + \tilde{t}_{(23)}^{(1)\beta} f_{(23)}^{(K^*)} \right] \quad (\text{A.5})$$

$$\langle \gamma 1^{++} | (a_0 \pi^0) 1 \rangle = \epsilon_{\mu\nu\alpha\beta} p_\psi^\alpha f_{(123)}^{(1^{++})} \tilde{t}_{(a_0\pi^0)}^{(1)\beta} f_{(12)}^{(a_0)} \quad (\text{A.6})$$

$$\langle \gamma 1^{++} | (a_0 \pi^0) 2 \rangle = q_\mu S_{\nu\beta} \tilde{t}_{(a_0\pi^0)}^{(1)\beta} B_2(Q_{\psi\gamma X}) f_{(123)}^{(1^{++})} f_{(12)}^{(a_0)} \quad (\text{A.7})$$

For the $J/\psi \rightarrow \gamma 2^{++}$ vertex, there are three independent couplings:

$$\begin{aligned} \langle \gamma 2^{++} | (K^* K) 1 \rangle &= P_{\mu\nu\alpha\beta}^{(2)}(K) \epsilon^{\alpha\lambda\gamma\sigma} K_\lambda f_{(123)}^{(2^{++})} \\ &\quad \times \left[\tilde{t}_{(K^*K)\gamma}^{(2)\beta} \tilde{t}_{(13)\sigma}^{(1)} f_{(13)}^{(K^*)} + \tilde{t}_{(K^*K)\gamma}^{(2)\beta} \tilde{t}_{(23)\sigma}^{(1)} f_{(23)}^{(K^*)} \right] \end{aligned} \quad (\text{A.8})$$

$$\begin{aligned} \langle \gamma 2^{++} | (K^* K) 2 \rangle &= g_{\mu\nu} p_\psi^\delta p_\psi^{\delta'} P_{\delta\delta'\alpha\beta}^{(2)}(K) \epsilon^{\alpha\lambda\gamma\sigma} K_\lambda f_{(123)}^{(2^{++})} \\ &\quad \times \left[\tilde{t}_{(K^*K)\gamma}^{(2)\beta} \tilde{t}_{(13)\sigma}^{(1)} f_{(13)}^{(K^*)} + \tilde{t}_{(K^*K)\gamma}^{(2)\beta} \tilde{t}_{(23)\sigma}^{(1)} f_{(23)}^{(K^*)} \right] B_2(Q_{\psi\gamma X}) \end{aligned} \quad (\text{A.9})$$

$$\begin{aligned} \langle \gamma 2^{++} | (K^* K) 3 \rangle &= q_\mu p_\psi^\delta P_{\nu\delta\alpha\beta}^{(2)}(K) \epsilon^{\alpha\lambda\gamma\sigma} K_\lambda f_{(123)}^{(2^{++})} \\ &\quad \times \left[\tilde{t}_{(K^*K)\gamma}^{(2)\beta} \tilde{t}_{(13)\sigma}^{(1)} f_{(13)}^{(K^*)} + \tilde{t}_{(K^*K)\gamma}^{(2)\beta} \tilde{t}_{(23)\sigma}^{(1)} f_{(23)}^{(K^*)} \right] B_2(Q_{\psi\gamma X}) \end{aligned} \quad (\text{A.10})$$

For the $J/\psi \rightarrow \gamma 2^{-+}$ vertex, there are three independent couplings:

$$\langle \gamma 2^{-+} | (a_0 \pi^0) 1 \rangle = \epsilon_{\mu\nu\alpha\beta} p_\psi^\alpha f_{(123)}^{(2^{-+})} \tilde{t}_{(a_0\pi^0)}^{(2)\beta\gamma} q_\gamma f_{(12)}^{(a_0)} B_1(Q_{\psi\gamma X}) \quad (\text{A.11})$$

$$\langle \gamma 2^{-+} | (a_0 \pi^0) 2 \rangle = S_{\mu\nu} p_\psi^\gamma p_\psi^\delta f_{(123)}^{(2^{-+})} \tilde{t}_{(a_0\pi^0)}^{(2)\gamma\delta} f_{(12)}^{(a_0)} B_3(Q_{\psi\gamma X}) \quad (\text{A.12})$$

$$\langle \gamma 2^{-+} | (a_0 \pi^0) 3 \rangle = q_\mu S_{\nu\gamma} f_{(123)}^{(2^{-+})} \tilde{t}_{(a_0\pi^0)}^{(2)\gamma\delta} p_\psi^\delta f_{(12)}^{(a_0)} B_3(Q_{\psi\gamma X}) \quad (\text{A.13})$$

here the partial-wave amplitudes are constructed with the pure-orbital-angular-momentum covariant tensors $\tilde{t}_{\mu_1 \dots \mu_l}^{(l)}$ and the covariant spin wave functions $\phi_{\mu_1 \dots \mu_l}$ together with the operators $g^{\mu\nu}$ and $\epsilon^{\mu\nu\alpha\beta}$. Besides, $P_{\mu_1 \dots \mu_S \mu'_1 \dots \mu'_S}^{(S)}(p_a)$ is the spin projection operator of meson a , B_l is the Blatt-Weisskopf barrier factor, the propagators of intermediate resonances are denoted as f and the $S_{\mu\nu}$ is defined as

$$S_{\mu\nu} = \epsilon_{\mu\nu\alpha\beta} p_\psi^\alpha q^\beta \quad (\text{A.14})$$

where p_ψ^α and q^β are the momenta of J/ψ and the radiative photon. More detailed derivation of the formulas, definitions of physical quantities and specific expressions have been given by the ref. [47].

Open Access. This article is distributed under the terms of the Creative Commons Attribution License ([CC-BY 4.0](https://creativecommons.org/licenses/by/4.0/)), which permits any use, distribution and reproduction in any medium, provided the original author(s) and source are credited. SCOAP³ supports the goals of the International Year of Basic Sciences for Sustainable Development.

References

- [1] D.L. Scharre et al., *Observation of the radiative transition $\psi \rightarrow \gamma E(1420)$* , *Phys. Lett. B* **97** (1980) 329 [[INSPIRE](#)].
- [2] C. Edwards et al., *Observation of a pseudoscalar state at 1440 MeV in J/ψ radiative decays*, *Phys. Rev. Lett.* **49** (1982) 259 [*Erratum ibid.* **50** (1983) 219] [[INSPIRE](#)].
- [3] A. Birman et al., *Partial wave analysis of the $K + \bar{K}^0\pi^-$ system*, *Phys. Rev. Lett.* **61** (1988) 1557 [*Erratum ibid.* **62** (1989) 1577] [[INSPIRE](#)].
- [4] OBELIX collaboration, *E/ι decays to $K\bar{K}\pi$ in $\bar{p}p$ annihilation at rest*, *Phys. Lett. B* **361** (1995) 187 [[INSPIRE](#)].
- [5] OBELIX collaboration, *Evidence for two pseudoscalar states in the 1.4 GeV to 1.5 GeV mass region*, *Phys. Lett. B* **462** (1999) 453 [[INSPIRE](#)].
- [6] OBELIX collaboration, *A search for axial vectors in $\bar{p}p \rightarrow K^\pm K_{\text{miss}}^0 \pi^\mp \pi^+ \pi^-$ annihilations at rest in gaseous hydrogen at NTP*, *Phys. Lett. B* **400** (1997) 226 [[INSPIRE](#)].
- [7] BES collaboration, *Partial wave analysis of $J/\psi \rightarrow \gamma(K^+K^-\pi^0)$* , *Phys. Lett. B* **440** (1998) 217 [[INSPIRE](#)].
- [8] DM2 collaboration, *Partial wave analysis of DM2 data in the $\eta(1430)$ energy range*, *Phys. Rev. D* **46** (1992) 1951 [[INSPIRE](#)].
- [9] CERN-COLLEGE DE FRANCE-MADRID-STOCKHOLM collaboration, *Observation and quantum numbers determination of the $E(1420)$ meson in π^-p interactions at 3.95 GeV/c*, *Nucl. Phys. B* **169** (1980) 1 [[INSPIRE](#)].
- [10] ATHENS-BARI-BIRMINGHAM-CERN collaboration, *Spin parity analysis of the E meson centrally produced in the reactions $\pi^+p \rightarrow \pi^+(K_L^0 K^\pm K^\mp)p$ and $pp \rightarrow p(K_L^0 K^\pm \pi^\mp)p$ at 85 GeV/c*, *Phys. Lett. B* **146** (1984) 273 [[INSPIRE](#)].
- [11] E852 collaboration, *Observation of pseudoscalar and axial vector resonances in $\pi^-p \rightarrow K^+K^-\pi^0n$ at 18 GeV*, *Phys. Lett. B* **516** (2001) 264 [[hep-ex/0107042](#)] [[INSPIRE](#)].
- [12] PARTICLE DATA GROUP collaboration, *Review of particle physics*, *PTEP* **2020** (2020) 083C01 [[INSPIRE](#)].
- [13] BES collaboration, *Partial wave analysis of $J/\psi \rightarrow \gamma(\eta\pi^+\pi^-)$* , *Phys. Lett. B* **446** (1999) 356 [[INSPIRE](#)].
- [14] E852 collaboration, *Partial-wave analysis of the $\eta\pi^+\pi^-$ system produced in the reaction $\pi^-p \rightarrow \eta\pi^+\pi^-n$ at 18 GeV/c*, *Phys. Rev. D* **62** (2000) 012003 [[hep-ex/0001051](#)] [[INSPIRE](#)].
- [15] BESIII collaboration, *Measurement of branching fractions of $\psi(3686) \rightarrow \phi\eta'$, $\phi f_1(1285)$ and $\phi\eta(1405)$* , *Phys. Rev. D* **100** (2019) 092003 [[arXiv:1906.00736](#)] [[INSPIRE](#)].
- [16] BESIII collaboration, *First observation of $\eta(1405)$ decays into $f_0(980)\pi^0$* , *Phys. Rev. Lett.* **108** (2012) 182001 [[arXiv:1201.2737](#)] [[INSPIRE](#)].

- [17] BESIII collaboration, *Study of $\eta(1475)$ and $X(1835)$ in radiative J/ψ decays to $\gamma\phi$* , *Phys. Rev. D* **97** (2018) 051101 [[arXiv:1801.02127](#)] [[INSPIRE](#)].
- [18] BES collaboration, *A study of $J/\psi \rightarrow \gamma\gamma V(\rho, \phi)$ decays with the BESII detector*, *Phys. Lett. B* **594** (2004) 47 [[hep-ex/0403008](#)] [[INSPIRE](#)].
- [19] J.D. Weinstein and N. Isgur, *The $qq\bar{q}\bar{q}$ system in a potential model*, *Phys. Rev. D* **27** (1983) 588 [[INSPIRE](#)].
- [20] J.D. Weinstein and N. Isgur, *$K\bar{K}$ molecules*, *Phys. Rev. D* **41** (1990) 2236 [[INSPIRE](#)].
- [21] R.S. Longacre, *The $e(1420)$ meson as a $K\bar{K}\pi$ molecule*, *Phys. Rev. D* **42** (1990) 874 [[INSPIRE](#)].
- [22] A. Masoni, *Pseudoscalar and axial vector meson production*, *Nucl. Phys. A* **655** (1999) 63 [[INSPIRE](#)].
- [23] G. Usai, *Pseudoscalar mesons in the $1\text{ GeV}/c^2$ to $2\text{ GeV}/c^2$ mass region*, *Nucl. Phys. A* **692** (2001) 315 [[INSPIRE](#)].
- [24] L. Faddeev, A.J. Niemi and U. Wiedner, *Glueballs, closed flux tubes and $\eta(1440)$* , *Phys. Rev. D* **70** (2004) 114033 [[hep-ph/0308240](#)] [[INSPIRE](#)].
- [25] H.-Y. Cheng, H.-N. Li and K.-F. Liu, *Pseudoscalar glueball mass from η - η' - G mixing*, *Phys. Rev. D* **79** (2009) 014024 [[arXiv:0811.2577](#)] [[INSPIRE](#)].
- [26] J.-J. Wu, X.-H. Liu, Q. Zhao and B.-S. Zou, *The puzzle of anomalously large isospin violations in $\eta(1405/1475) \rightarrow 3\pi$* , *Phys. Rev. Lett.* **108** (2012) 081803 [[arXiv:1108.3772](#)] [[INSPIRE](#)].
- [27] X.-G. Wu, J.-J. Wu, Q. Zhao and B.-S. Zou, *Understanding the property of $\eta(1405/1475)$ in the J/ψ radiative decay*, *Phys. Rev. D* **87** (2013) 014023 [[arXiv:1211.2148](#)] [[INSPIRE](#)].
- [28] M.-C. Du and Q. Zhao, *Internal particle width effects on the triangle singularity mechanism in the study of the $\eta(1405)$ and $\eta(1475)$ puzzle*, *Phys. Rev. D* **100** (2019) 036005 [[arXiv:1905.04207](#)] [[INSPIRE](#)].
- [29] M.-C. Du and Q. Zhao, *Comprehensive study of light axial vector mesons with the presence of triangle singularity*, *Phys. Rev. D* **104** (2021) 036008 [[arXiv:2103.16861](#)] [[INSPIRE](#)].
- [30] BESIII collaboration, *Number of J/ψ events at BESIII*, *Chin. Phys. C* **46** (2022) 074001 [[arXiv:2111.07571](#)] [[INSPIRE](#)].
- [31] BESIII collaboration, *Design and construction of the BESIII detector*, *Nucl. Instrum. Meth. A* **614** (2010) 345 [[arXiv:0911.4960](#)] [[INSPIRE](#)].
- [32] C. Yu et al., *BEPCII performance and beam dynamics studies on luminosity*, in the proceedings of 7th international particle accelerator conference, (2016), p. TUYA01 [[DOI:10.18429/JACoW-IPAC2016-TUYA01](#)] [[INSPIRE](#)].
- [33] BESIII collaboration, *Future physics programme of BESIII*, *Chin. Phys. C* **44** (2020) 040001 [[arXiv:1912.05983](#)] [[INSPIRE](#)].
- [34] X. Li et al., *Study of MRPC technology for BESIII endcap-TOF upgrade*, *Radiat. Detect. Technol. Meth.* **1** (2017) 13.
- [35] Y.-X. Guo et al., *The study of time calibration for upgraded end cap TOF of BESIII*, *Radiat. Detect. Technol. Meth.* **1** (2017) 15.

- [36] GEANT4 collaboration, *GEANT4 — a simulation toolkit*, *Nucl. Instrum. Meth. A* **506** (2003) 250 [INSPIRE].
- [37] Y.-T. Liang et al., *A uniform geometry description for simulation, reconstruction and visualization in the BESIII experiment*, *Nucl. Instrum. Meth. A* **603** (2009) 325 [INSPIRE].
- [38] Y. Zheng-Yun, L. Yu-Tie and M. Ya-Jun, *A method for detector description exchange among ROOT GEANT4 and GEANT3*, *Chin. Phys. C* **32** (2008) 572.
- [39] S. Jadach, B.F.L. Ward and Z. Was, *Coherent exclusive exponentiation for precision Monte Carlo calculations*, *Nucl. Phys. B Proc. Suppl.* **89** (2000) 106 [hep-ph/0012124] [INSPIRE].
- [40] S. Jadach, B.F.L. Ward and Z. Was, *The precision Monte Carlo event generator KK for two fermion final states in e^+e^- collisions*, *Comput. Phys. Commun.* **130** (2000) 260 [hep-ph/9912214] [INSPIRE].
- [41] D.J. Lange, *The EvtGen particle decay simulation package*, *Nucl. Instrum. Meth. A* **462** (2001) 152 [INSPIRE].
- [42] R.-G. Ping, *Event generators at BESIII*, *Chin. Phys. C* **32** (2008) 599 [INSPIRE].
- [43] R.-L. Yang, R.-G. Ping and H. Chen, *Tuning and validation of the Lundcharm model with J/ψ decays*, *Chin. Phys. Lett.* **31** (2014) 061301 [INSPIRE].
- [44] J.C. Chen et al., *Event generator for J/ψ and $\psi(2S)$ decay*, *Phys. Rev. D* **62** (2000) 034003 [INSPIRE].
- [45] E. Richter-Was, *QED bremsstrahlung in semileptonic B and leptonic τ decays*, *Phys. Lett. B* **303** (1993) 163 [INSPIRE].
- [46] N. Berger, B. Liu and J. Wang, *Partial wave analysis using graphics processing units*, *J. Phys. Conf. Ser.* **219** (2010) 042031 [INSPIRE].
- [47] B.S. Zou and D.V. Bugg, *Covariant tensor formalism for partial wave analyses of ψ decay to mesons*, *Eur. Phys. J. A* **16** (2003) 537 [hep-ph/0211457] [INSPIRE].
- [48] D.V. Bugg, *Re-analysis of data on $a_0(1450)$ and $a_0(980)$* , *Phys. Rev. D* **78** (2008) 074023 [arXiv:0808.2706] [INSPIRE].
- [49] BESIII collaboration, *Amplitude analysis of the $\chi_{c1} \rightarrow \eta\pi^+\pi^-$ decays*, *Phys. Rev. D* **95** (2017) 032002 [arXiv:1610.02479] [INSPIRE].
- [50] BESIII collaboration, *Observation of pseudoscalar and tensor resonances in $J/\psi \rightarrow \gamma\phi\phi$* , *Phys. Rev. D* **93** (2016) 112011 [arXiv:1602.01523] [INSPIRE].
- [51] F. James and M. Roos, *Minuit: a system for function minimization and analysis of the parameter errors and correlations*, *Comput. Phys. Commun.* **10** (1975) 343 [INSPIRE].
- [52] BES collaboration, *Partial wave analyses of $J/\psi \rightarrow \gamma K^+K^-$ and $\gamma K_S^0 K_S^0$* , *Phys. Rev. D* **68** (2003) 052003 [hep-ex/0307058] [INSPIRE].
- [53] BESIII collaboration, *Branching fraction measurements of χ_{c0} and χ_{c2} to $\pi^0\pi^0$ and $\eta\eta$* , *Phys. Rev. D* **81** (2010) 052005 [arXiv:1001.5360] [INSPIRE].
- [54] BESIII collaboration, *Observation and spin-parity determination of the $X(1835)$ in $J/\psi \rightarrow \gamma K_S^0 K_S^0 \eta$* , *Phys. Rev. Lett.* **115** (2015) 091803 [arXiv:1506.04807] [INSPIRE].
- [55] BESIII collaboration, *Search for hadronic transition $\chi_{cJ} \rightarrow \eta_c\pi^+\pi^-$ and observation of $\chi_{cJ} \rightarrow K\bar{K}\pi\pi\pi$* , *Phys. Rev. D* **87** (2013) 012002 [arXiv:1208.4805] [INSPIRE].
- [56] F. Von Hippel and C. Quigg, *Centrifugal-barrier effects in resonance partial decay widths, shapes, and production amplitudes*, *Phys. Rev. D* **5** (1972) 624 [INSPIRE].

The BESIII collaboration

M. Ablikim¹, M. N. Achasov^{11,b}, P. Adlarson⁷⁰, M. Albrecht⁴, R. Aliberti³¹, A. Amoroso^{69A,69C}, M. R. An³⁵, Q. An^{66,53}, X. H. Bai⁶¹, Y. Bai⁵², O. Bakina³², R. Baldini Ferroli^{26A}, I. Balossino^{27A}, Y. Ban^{42,g}, V. Batozskaya^{1,40}, D. Becker³¹, K. Begzsuren²⁹, N. Berger³¹, M. Bertani^{26A}, D. Bettoni^{27A}, F. Bianchi^{69A,69C}, J. Bloms⁶³, A. Bortone^{69A,69C}, I. Boyko³², R. A. Briere⁵, A. Brueggemann⁶³, H. Cai⁷¹, X. Cai^{1,53}, A. Calcaterra^{26A}, G. F. Cao^{1,58}, N. Cao^{1,58}, S. A. Cetin^{57A}, J. F. Chang^{1,53}, W. L. Chang^{1,58}, G. Chelkov^{32,a}, C. Chen³⁹, Chao Chen⁵⁰, G. Chen¹, H. S. Chen^{1,58}, M. L. Chen^{1,53}, S. J. Chen³⁸, S. M. Chen⁵⁶, T. Chen¹, X. R. Chen^{28,58}, X. T. Chen¹, Y. B. Chen^{1,53}, Z. J. Chen^{23,h}, W. S. Cheng^{69C}, S. K. Choi⁵⁰, X. Chu³⁹, G. Cibinetto^{27A}, F. Cossio^{69C}, J. J. Cui⁴⁵, H. L. Dai^{1,53}, J. P. Dai⁷³, A. Dbeyssi¹⁷, R. E. de Boer⁴, D. Dedovich³², Z. Y. Deng¹, A. Denig³¹, I. Denysenko³², M. Destefanis^{69A,69C}, F. De Mori^{69A,69C}, Y. Ding³⁶, J. Dong^{1,53}, L. Y. Dong^{1,58}, M. Y. Dong^{1,53,58}, X. Dong⁷¹, S. X. Du⁷⁵, P. Egorov^{32,a}, Y. L. Fan⁷¹, J. Fang^{1,53}, S. S. Fang^{1,58}, W. X. Fang¹, Y. Fang¹, R. Farinelli^{27A}, L. Fava^{69B,69C}, F. Feldbauer⁴, G. Felici^{26A}, C. Q. Feng^{66,53}, J. H. Feng⁵⁴, K. Fischer⁶⁴, M. Fritsch⁴, C. Fritsch⁶³, C. D. Fu¹, H. Gao⁵⁸, Y. N. Gao^{42,g}, Yang Gao^{66,53}, S. Garbolino^{69C}, I. Garzia^{27A,27B}, P. T. Ge⁷¹, Z. W. Ge³⁸, C. Geng⁵⁴, E. M. Gersabeck⁶², A. Gilman⁶⁴, K. Goetzen¹², L. Gong³⁶, W. X. Gong^{1,53}, W. Gradl³¹, M. Greco^{69A,69C}, L. M. Gu³⁸, M. H. Gu^{1,53}, Y. T. Gu¹⁴, C. Y. Guan^{1,58}, A. Q. Guo^{28,58}, L. B. Guo³⁷, R. P. Guo⁴⁴, Y. P. Guo^{10,f}, A. Guskov^{32,a}, T. T. Han⁴⁵, W. Y. Han³⁵, X. Q. Hao¹⁸, F. A. Harris⁶⁰, K. K. He⁵⁰, K. L. He^{1,58}, F. H. Heinsius⁴, C. H. Heinz³¹, Y. K. Heng^{1,53,58}, C. Herold⁵⁵, M. Himmelreich^{31,d}, G. Y. Hou^{1,58}, Y. R. Hou⁵⁸, Z. L. Hou¹, H. M. Hu^{1,58}, J. F. Hu^{51,i}, T. Hu^{1,53,58}, Y. Hu¹, G. S. Huang^{66,53}, K. X. Huang⁵⁴, L. Q. Huang⁶⁷, L. Q. Huang^{28,58}, X. T. Huang⁴⁵, Y. P. Huang¹, Z. Huang^{42,g}, T. Hussain⁶⁸, N. Hüsken^{25,31}, W. Imoehl²⁵, M. Irshad^{66,53}, J. Jackson²⁵, S. Jaeger⁴, S. Janchiv²⁹, E. Jang⁵⁰, J. H. Jeong⁵⁰, Q. Ji¹, Q. P. Ji¹⁸, X. B. Ji^{1,58}, X. L. Ji^{1,53}, Y. Y. Ji⁴⁵, Z. K. Jia^{66,53}, H. B. Jiang⁴⁵, S. S. Jiang³⁵, X. S. Jiang^{1,53,58}, Y. Jiang⁵⁸, Yi Jiang^{66,53}, J. B. Jiao⁴⁵, Z. Jiao²¹, S. Jin³⁸, Y. Jin⁶¹, M. Q. Jing^{1,58}, T. Johansson⁷⁰, N. Kalantar-Nayestanaki⁵⁹, X. S. Kang³⁶, R. Kappert⁵⁹, B. C. Ke⁷⁵, I. K. Keshk⁴, A. Khoukaz⁶³, R. Kiuchi¹, R. Kliemt¹², L. Koch³³, O. B. Kolcu^{57A}, B. Kopf⁴, M. Kuemmel⁴, M. Kuessner⁴, A. Kupsc^{40,70}, W. Kühn³³, J. J. Lane⁶², J. S. Lange³³, P. Larin¹⁷, A. Lavania²⁴, L. Lavezzi^{69A,69C}, Z. H. Lei^{66,53}, H. Leithoff³¹, M. Lellmann³¹, T. Lenz³¹, C. Li³⁹, C. Li⁴³, C. H. Li³⁵, Cheng Li^{66,53}, D. M. Li⁷⁵, F. Li^{1,53}, G. Li¹, H. Li^{66,53}, H. Li⁴⁷, H. B. Li^{1,58}, H. J. Li¹⁸, H. N. Li^{51,i}, J. Q. Li⁴, J. S. Li⁵⁴, J. W. Li⁴⁵, Ke Li¹, L. J Li¹, L. K. Li¹, Lei Li³, M. H. Li³⁹, P. R. Li^{34,j,k}, S. X. Li¹⁰, S. Y. Li⁵⁶, T. Li⁴⁵, W. D. Li^{1,58}, W. G. Li¹, X. H. Li^{66,53}, X. L. Li⁴⁵, Xiaoyu Li^{1,58}, Z. X. Li¹⁴, H. Liang^{66,53}, H. Liang³⁰, H. Liang^{1,58}, Y. F. Liang⁴⁹, Y. T. Liang^{28,58}, G. R. Liao¹³, L. Z. Liao⁴⁵, J. Libby²⁴, A. Limphirat⁵⁵, C. X. Lin⁵⁴, D. X. Lin^{28,58}, T. Lin¹, B. J. Liu¹, C. X. Liu¹, D. Liu^{17,66}, F. H. Liu⁴⁸, Fang Liu¹, Feng Liu⁶, G. M. Liu^{51,i}, H. Liu^{34,j,k}, H. B. Liu¹⁴, H. M. Liu^{1,58}, Huanhuan Liu¹, Huihui Liu¹⁹, J. B. Liu^{66,53}, J. L. Liu⁶⁷, J. Y. Liu^{1,58}, K. Liu¹, K. Y. Liu³⁶, Ke Liu²⁰, L. Liu^{66,53}, Lu Liu³⁹, M. H. Liu^{10,f}, P. L. Liu¹, Q. Liu⁵⁸, S. B. Liu^{66,53}, T. Liu^{10,f}, W. K. Liu³⁹, W. M. Liu^{66,53}, X. Liu^{34,j,k}, Y. Liu^{34,j,k}, Y. B. Liu³⁹, Z. A. Liu^{1,53,58}, Z. Q. Liu⁴⁵, X. C. Lou^{1,53,58}, F. X. Lu⁵⁴, H. J. Lu²¹, J. G. Lu^{1,53}, X. L. Lu¹, Y. Lu⁷, Y. P. Lu^{1,53}, Z. H. Lu¹, C. L. Luo³⁷, M. X. Luo⁷⁴, T. Luo^{10,f}, X. L. Luo^{1,53}, X. R. Lyu⁵⁸, Y. F. Lyu³⁹, F. C. Ma³⁶, H. L. Ma¹, L. L. Ma⁴⁵, M. M. Ma^{1,58}, Q. M. Ma¹, R. Q. Ma^{1,58}, R. T. Ma⁵⁸, X. Y. Ma^{1,53}, Y. Ma^{42,g}, F. E. Maas¹⁷, M. Maggiora^{69A,69C}, S. Maldaner⁴, S. Malde⁶⁴, Q. A. Malik⁶⁸, A. Mangoni^{26B}, Y. J. Mao^{42,g}, Z. P. Mao¹, S. Marcello^{69A,69C}, Z. X. Meng⁶¹, G. Mezzadri^{27A}, H. Miao¹, T. J. Min³⁸, R. E. Mitchell²⁵, X. H. Mo^{1,53,58}, N. Yu. Muchnoi^{11,b}, Y. Nefedov³², F. Nerling^{17,d}, I. B. Nikolaev^{11,b}, Z. Ning^{1,53}, S. Nisar^{9,l}, Y. Niu⁴⁵, S. L. Olsen⁵⁸, Q. Ouyang^{1,53,58}, S. Pacetti^{26B,26C}, X. Pan^{10,f}, Y. Pan⁵², A. Pathak³⁰, M. Pelizaeus⁴, H. P. Peng^{66,53},

K. Peters^{12,d}, J. L. Ping³⁷, R. G. Ping^{1,58}, S. Plura³¹, S. Pogodin³², V. Prasad^{66,53}, F. Z. Qi¹, H. Qi^{66,53}, H. R. Qi⁵⁶, M. Qi³⁸, T. Y. Qi^{10,f}, S. Qian^{1,53}, W. B. Qian⁵⁸, Z. Qian⁵⁴, C. F. Qiao⁵⁸, J. J. Qin⁶⁷, L. Q. Qin¹³, X. P. Qin^{10,f}, X. S. Qin⁴⁵, Z. H. Qin^{1,53}, J. F. Qiu¹, S. Q. Qu⁵⁶, K. H. Rashid⁶⁸, C. F. Redmer³¹, K. J. Ren³⁵, A. Rivetti^{69C}, V. Rodin⁵⁹, M. Rolo^{69C}, G. Rong^{1,58}, Ch. Rosner¹⁷, S. N. Ruan³⁹, H. S. Sang⁶⁶, A. Sarantsev^{32,c}, Y. Schelhaas³¹, C. Schmier⁴, K. Schoenning⁷⁰, M. Scodeggio^{27A,27B}, K. Y. Shan^{10,f}, W. Shan²², X. Y. Shan^{66,53}, J. F. Shangguan⁵⁰, L. G. Shao^{1,58}, M. Shao^{66,53}, C. P. Shen^{10,f}, H. F. Shen^{1,58}, X. Y. Shen^{1,58}, B. A. Shi⁵⁸, H. C. Shi^{66,53}, J. Y. Shi¹, Q. Q. Shi⁵⁰, R. S. Shi^{1,58}, X. Shi^{1,53}, X. D Shi^{66,53}, J. J. Song¹⁸, W. M. Song^{30,1}, Y. X. Song^{42,g}, S. Sosio^{69A,69C}, S. Spataro^{69A,69C}, F. Stieler³¹, K. X. Su⁷¹, P. P. Su⁵⁰, Y. J. Su⁵⁸, G. X. Sun¹, H. Sun⁵⁸, H. K. Sun¹, J. F. Sun¹⁸, L. Sun⁷¹, S. S. Sun^{1,58}, T. Sun^{1,58}, W. Y. Sun³⁰, X Sun^{23,h}, Y. J. Sun^{66,53}, Y. Z. Sun¹, Z. T. Sun⁴⁵, Y. H. Tan⁷¹, Y. X. Tan^{66,53}, C. J. Tang⁴⁹, G. Y. Tang¹, J. Tang⁵⁴, L. Y Tao⁶⁷, Q. T. Tao^{23,h}, M. Tat⁶⁴, J. X. Teng^{66,53}, V. Thoren⁷⁰, W. H. Tian⁴⁷, Y. Tian^{28,58}, I. Uman^{57B}, B. Wang¹, B. L. Wang⁵⁸, C. W. Wang³⁸, D. Y. Wang^{42,g}, F. Wang⁶⁷, H. J. Wang^{34,j,k}, H. P. Wang^{1,58}, K. Wang^{1,53}, L. L. Wang¹, M. Wang⁴⁵, M. Z. Wang^{42,g}, Meng Wang^{1,58}, S. Wang^{10,f}, S. Wang¹³, T. Wang^{10,f}, T. J. Wang³⁹, W. Wang⁵⁴, W. H. Wang⁷¹, W. P. Wang^{66,53}, X. Wang^{42,g}, X. F. Wang^{34,j,k}, X. L. Wang^{10,f}, Y. Wang⁵⁶, Y. D. Wang⁴¹, Y. F. Wang^{1,53,58}, Y. H. Wang⁴³, Y. Q. Wang¹, Yaqian Wang^{16,1}, Z. Wang^{1,53}, Z. Y. Wang^{1,58}, Ziyi Wang⁵⁸, D. H. Wei¹³, F. Weidner⁶³, S. P. Wen¹, D. J. White⁶², U. Wiedner⁴, G. Wilkinson⁶⁴, M. Wolke⁷⁰, L. Wollenberg⁴, J. F. Wu^{1,58}, L. H. Wu¹, L. J. Wu^{1,58}, X. Wu^{10,f}, X. H. Wu³⁰, Y. Wu⁶⁶, Z. Wu^{1,53}, L. Xia^{66,53}, T. Xiang^{42,g}, D. Xiao^{34,j,k}, G. Y. Xiao³⁸, H. Xiao^{10,f}, S. Y. Xiao¹, Y. L. Xiao^{10,f}, Z. J. Xiao³⁷, C. Xie³⁸, X. H. Xie^{42,g}, Y. Xie⁴⁵, Y. G. Xie^{1,53}, Y. H. Xie⁶, Z. P. Xie^{66,53}, T. Y. Xing^{1,58}, C. F. Xu¹, C. J. Xu⁵⁴, G. F. Xu¹, H. Y. Xu⁶¹, Q. J. Xu¹⁵, X. P. Xu⁵⁰, Y. C. Xu⁵⁸, Z. P. Xu³⁸, F. Yan^{10,f}, L. Yan^{10,f}, W. B. Yan^{66,53}, W. C. Yan⁷⁵, H. J. Yang^{46,e}, H. L. Yang³⁰, H. X. Yang¹, L. Yang⁴⁷, S. L. Yang⁵⁸, Tao Yang¹, Y. F. Yang³⁹, Y. X. Yang^{1,58}, Yifan Yang^{1,58}, M. Ye^{1,53}, M. H. Ye⁸, J. H. Yin¹, Z. Y. You⁵⁴, B. X. Yu^{1,53,58}, C. X. Yu³⁹, G. Yu^{1,58}, T. Yu⁶⁷, X. D. Yu^{42,g}, C. Z. Yuan^{1,58}, L. Yuan², S. C. Yuan¹, X. Q. Yuan¹, Y. Yuan^{1,58}, Z. Y. Yuan⁵⁴, C. X. Yue³⁵, A. A. Zafar⁶⁸, F. R. Zeng⁴⁵, X. Zeng⁶, Y. Zeng^{23,h}, Y. H. Zhan⁵⁴, A. Q. Zhang¹, B. L. Zhang¹, B. X. Zhang¹, D. H. Zhang³⁹, G. Y. Zhang¹⁸, H. Zhang⁶⁶, H. H. Zhang⁵⁴, H. H. Zhang³⁰, H. Y. Zhang^{1,53}, J. L. Zhang⁷², J. Q. Zhang³⁷, J. W. Zhang^{1,53,58}, J. X. Zhang^{34,j,k}, J. Y. Zhang¹, J. Z. Zhang^{1,58}, Jianyu Zhang^{1,58}, Jiawei Zhang^{1,58}, L. M. Zhang⁵⁶, L. Q. Zhang⁵⁴, Lei Zhang³⁸, P. Zhang¹, Q. Y. Zhang^{35,75}, Shuihan Zhang^{1,58}, Shulei Zhang^{23,h}, X. D. Zhang⁴¹, X. M. Zhang¹, X. Y. Zhang⁴⁵, X. Y. Zhang⁵⁰, Y. Zhang⁶⁴, Y. T. Zhang⁷⁵, Y. H. Zhang^{1,53}, Yan Zhang^{66,53}, Yao Zhang¹, Z. H. Zhang¹, Z. Y. Zhang³⁹, Z. Y. Zhang⁷¹, G. Zhao¹, J. Zhao³⁵, J. Y. Zhao^{1,58}, J. Z. Zhao^{1,53}, Lei Zhao^{66,53}, Ling Zhao¹, M. G. Zhao³⁹, Q. Zhao¹, S. J. Zhao⁷⁵, Y. B. Zhao^{1,53}, Y. X. Zhao^{28,58}, Z. G. Zhao^{66,53}, A. Zhemchugov^{32,a}, B. Zheng⁶⁷, J. P. Zheng^{1,53}, Y. H. Zheng⁵⁸, B. Zhong³⁷, C. Zhong⁶⁷, X. Zhong⁵⁴, H. Zhou⁴⁵, L. P. Zhou^{1,58}, X. Zhou⁷¹, X. K. Zhou⁵⁸, X. R. Zhou^{66,53}, X. Y. Zhou³⁵, Y. Z. Zhou^{10,f}, J. Zhu³⁹, K. Zhu¹, K. J. Zhu^{1,53,58}, L. X. Zhu⁵⁸, S. H. Zhu⁶⁵, S. Q. Zhu³⁸, T. J. Zhu⁷², W. J. Zhu^{10,f}, Y. C. Zhu^{66,53}, Z. A. Zhu^{1,58}, B. S. Zou¹ and J. H. Zou¹

¹ Institute of High Energy Physics, Beijing 100049, People's Republic of China

² Beihang University, Beijing 100191, People's Republic of China

³ Beijing Institute of Petrochemical Technology, Beijing 102617, People's Republic of China

⁴ Bochum Ruhr-University, D-44780 Bochum, Germany

⁵ Carnegie Mellon University, Pittsburgh, Pennsylvania 15213, U.S.A.

⁶ Central China Normal University, Wuhan 430079, People's Republic of China

⁷ Central South University, Changsha 410083, People's Republic of China

⁸ China Center of Advanced Science and Technology, Beijing 100190, People's Republic of China

- ⁹ COMSATS University Islamabad, Lahore Campus, Defence Road, Off Raiwind Road, 54000 Lahore, Pakistan
- ¹⁰ Fudan University, Shanghai 200433, People's Republic of China
- ¹¹ G.I. Budker Institute of Nuclear Physics SB RAS (BINP), Novosibirsk 630090, Russia
- ¹² GSI Helmholtzcentre for Heavy Ion Research GmbH, D-64291 Darmstadt, Germany
- ¹³ Guangxi Normal University, Guilin 541004, People's Republic of China
- ¹⁴ Guangxi University, Nanning 530004, People's Republic of China
- ¹⁵ Hangzhou Normal University, Hangzhou 310036, People's Republic of China
- ¹⁶ Hebei University, Baoding 071002, People's Republic of China
- ¹⁷ Helmholtz Institute Mainz, Staudinger Weg 18, D-55099 Mainz, Germany
- ¹⁸ Henan Normal University, Xinxiang 453007, People's Republic of China
- ¹⁹ Henan University of Science and Technology, Luoyang 471003, People's Republic of China
- ²⁰ Henan University of Technology, Zhengzhou 450001, People's Republic of China
- ²¹ Huangshan College, Huangshan 245000, People's Republic of China
- ²² Hunan Normal University, Changsha 410081, People's Republic of China
- ²³ Hunan University, Changsha 410082, People's Republic of China
- ²⁴ Indian Institute of Technology Madras, Chennai 600036, India
- ²⁵ Indiana University, Bloomington, Indiana 47405, U.S.A.
- ²⁶ INFN Laboratori Nazionali di Frascati , (A)INFN Laboratori Nazionali di Frascati, I-00044, Frascati, Italy; (B)INFN Sezione di Perugia, I-06100, Perugia, Italy; (C)University of Perugia, I-06100, Perugia, Italy
- ²⁷ INFN Sezione di Ferrara, (A)INFN Sezione di Ferrara, I-44122, Ferrara, Italy; (B)University of Ferrara, I-44122, Ferrara, Italy
- ²⁸ Institute of Modern Physics, Lanzhou 730000, People's Republic of China
- ²⁹ Institute of Physics and Technology, Peace Avenue 54B, Ulaanbaatar 13330, Mongolia
- ³⁰ Jilin University, Changchun 130012, People's Republic of China
- ³¹ Johannes Gutenberg University of Mainz, Johann-Joachim-Becher-Weg 45, D-55099 Mainz, Germany
- ³² Joint Institute for Nuclear Research, 141980 Dubna, Moscow region, Russia
- ³³ Justus-Liebig-Universitaet Giessen, II. Physikalisches Institut, Heinrich-Buff-Ring 16, D-35392 Giessen, Germany
- ³⁴ Lanzhou University, Lanzhou 730000, People's Republic of China
- ³⁵ Liaoning Normal University, Dalian 116029, People's Republic of China
- ³⁶ Liaoning University, Shenyang 110036, People's Republic of China
- ³⁷ Nanjing Normal University, Nanjing 210023, People's Republic of China
- ³⁸ Nanjing University, Nanjing 210093, People's Republic of China
- ³⁹ Nankai University, Tianjin 300071, People's Republic of China
- ⁴⁰ National Centre for Nuclear Research, Warsaw 02-093, Poland
- ⁴¹ North China Electric Power University, Beijing 102206, People's Republic of China
- ⁴² Peking University, Beijing 100871, People's Republic of China
- ⁴³ Qufu Normal University, Qufu 273165, People's Republic of China
- ⁴⁴ Shandong Normal University, Jinan 250014, People's Republic of China
- ⁴⁵ Shandong University, Jinan 250100, People's Republic of China
- ⁴⁶ Shanghai Jiao Tong University, Shanghai 200240, People's Republic of China
- ⁴⁷ Shanxi Normal University, Linfen 041004, People's Republic of China
- ⁴⁸ Shanxi University, Taiyuan 030006, People's Republic of China
- ⁴⁹ Sichuan University, Chengdu 610064, People's Republic of China
- ⁵⁰ Soochow University, Suzhou 215006, People's Republic of China
- ⁵¹ South China Normal University, Guangzhou 510006, People's Republic of China
- ⁵² Southeast University, Nanjing 211100, People's Republic of China
- ⁵³ State Key Laboratory of Particle Detection and Electronics, Beijing 100049, Hefei 230026, People's Republic of China

- ⁵⁴ Sun Yat-Sen University, Guangzhou 510275, People's Republic of China
- ⁵⁵ Suranaree University of Technology, University Avenue 111, Nakhon Ratchasima 30000, Thailand
- ⁵⁶ Tsinghua University, Beijing 100084, People's Republic of China
- ⁵⁷ Turkish Accelerator Center Particle Factory Group, (A)Istinye University, 34010, Istanbul, Turkey; (B)Near East University, Nicosia, North Cyprus, Mersin 10, Turkey
- ⁵⁸ University of Chinese Academy of Sciences, Beijing 100049, People's Republic of China
- ⁵⁹ University of Groningen, NL-9747 AA Groningen, The Netherlands
- ⁶⁰ University of Hawaii, Honolulu, Hawaii 96822, U.S.A.
- ⁶¹ University of Jinan, Jinan 250022, People's Republic of China
- ⁶² University of Manchester, Oxford Road, Manchester, M13 9PL, United Kingdom
- ⁶³ University of Muenster, Wilhelm-Klemm-Strasse 9, 48149 Muenster, Germany
- ⁶⁴ University of Oxford, Keble Road, Oxford OX13RH, United Kingdom
- ⁶⁵ University of Science and Technology Liaoning, Anshan 114051, People's Republic of China
- ⁶⁶ University of Science and Technology of China, Hefei 230026, People's Republic of China
- ⁶⁷ University of South China, Hengyang 421001, People's Republic of China
- ⁶⁸ University of the Punjab, Lahore-54590, Pakistan
- ⁶⁹ University of Turin and INFN, (A)University of Turin, I-10125, Turin, Italy; (B)University of Eastern Piedmont, I-15121, Alessandria, Italy; (C)INFN, I-10125, Turin, Italy
- ⁷⁰ Uppsala University, Box 516, SE-75120 Uppsala, Sweden
- ⁷¹ Wuhan University, Wuhan 430072, People's Republic of China
- ⁷² Xinyang Normal University, Xinyang 464000, People's Republic of China
- ⁷³ Yunnan University, Kunming 650500, People's Republic of China
- ⁷⁴ Zhejiang University, Hangzhou 310027, People's Republic of China
- ⁷⁵ Zhengzhou University, Zhengzhou 450001, People's Republic of China
- ^a Also at the Moscow Institute of Physics and Technology, Moscow 141700, Russia
- ^b Also at the Novosibirsk State University, Novosibirsk, 630090, Russia
- ^c Also at the NRC "Kurchatov Institute", PNPI, 188300, Gatchina, Russia
- ^d Also at Goethe University Frankfurt, 60323 Frankfurt am Main, Germany
- ^e Also at Key Laboratory for Particle Physics, Astrophysics and Cosmology, Ministry of Education; Shanghai Key Laboratory for Particle Physics and Cosmology; Institute of Nuclear and Particle Physics, Shanghai 200240, People's Republic of China
- ^f Also at Key Laboratory of Nuclear Physics and Ion-beam Application (MOE) and Institute of Modern Physics, Fudan University, Shanghai 200443, People's Republic of China
- ^g Also at State Key Laboratory of Nuclear Physics and Technology, Peking University, Beijing 100871, People's Republic of China
- ^h Also at School of Physics and Electronics, Hunan University, Changsha 410082, China
- ⁱ Also at Guangdong Provincial Key Laboratory of Nuclear Science, Institute of Quantum Matter, South China Normal University, Guangzhou 510006, China
- ^j Also at Frontiers Science Center for Rare Isotopes, Lanzhou University, Lanzhou 730000, People's Republic of China
- ^k Also at Lanzhou Center for Theoretical Physics, Lanzhou University, Lanzhou 730000, People's Republic of China
- ^l Also at the Department of Mathematical Sciences, IBA, Karachi, Pakistan